NASA CR-135355

DEVELOPMENT OF PROCEDURES FOR CALCULATING STIFFNESS AND DAMPING PROPERTIES OF ELASTOMERS IN ENGINEERING APPLICATIONS

Part IV. Testing of Elastomers Under a Rotating Load

By: M. S. Darlow and A. J. Smalley

MECHANICAL TECHNOLOGY INCORPORATED

Prepared for
NATIONAL AERONAUTICS AND SPACE ADMINISTRATION

NASA Lewis Research Center
Contract NAS 3-18546

1. Report No. NASA CR-135355	2. Government Accession No.	3. Recipient's Catalog No.
4. Title and Subtitle DEVELOPMENT OF PROCEDURES FOR CALCULATING STIFFNESS AND DAMPING PROPERTIES OF ELASTOMERS IN ENGINEERING APPLICATIONS. PART IV - TESTING OF ELASTOMERS UNDER A ROTATING LOAD		5. Report Date NOVEMBER 1977 6. Performing Organization Code
7. Author(s) M. S. Darlow, A. J. Smalley		8. Performing Organization Report No. MTI 78TR18 10. Work Unit No.
9. Performing Organization Name and Address MECHANICAL TECHNOLOGY INCORPORATED 968 ALBANY-SHAKER ROAD LATHAM, NEW YORK 12110		11. Contract or Grant No. NAS 3-18546 13. Type of Report and Period Covered CONTRACTOR REPORT
12. Sponsoring Agency Name and Address National Aeronautics and Space Administration Washington, D.C. 20546		14. Sponsoring Agency Code

15. Supplementary Notes
FINAL REPORT
Project Manager Robert E. Cunningham
Fluid Systems Components
NASA Lewis Research Center
Cleveland, Ohio 44135

16. Abstract

A test rig designed to measure stiffness and damping of elastomer cartridges under a rotating load excitation is described. The test rig employs rotating unbalance in a rotor which runs to 60,000 RPM as the excitation mechanism. A variable resonant mass is supported on elastomer elements and the dynamic characteristics are determined from measurements of input and output acceleration.

Five different cartridges are considered: three of these are buttons cartridges having buttons located in pairs, with 120° between each pair. Two of the cartridges consist of 360° elastomer rings with rectanglar cross-sections.

Dynamic stiffness and damping are measured for each cartridge and compared with predictions at different frequencies and different strains.

17. Key Words (Suggested by Author(s))	18. Distribution Statement
Viscoelasticity Elastomers Dynamic Properties Damping Vibrations Critical Speeds Resonance Testing	Unclassified, Unlimited

19. Security Classif. (of this report)	20. Security Classif. (of this page)	21. No. of Pages	22. Price*
Unclassified	Unclassified	97	

* For sale by the National Technical Information Service, Springfield, Virginia 22161

NASA-C-168 (Rev. 10-75)

FOREWORD

This report presents the work performed under NASA contract NAS3-18546 in the period October, 1975 to March, 1977, with Mr. Robert E. Cunningham, NASA Lewis Research Center as Project Manager. It is the fourth in a series of reports on the development of procedures for calculating stiffness and damping properties of elastomers in engineering applications. The Program Manager for MTI was Dr. A. J. Smalley. Principal Investigator for the experimental portions was Mr. M. S. Darlow. The analysis for reduction of test data was developed by Dr. P. K. Gupta. Mr. D. A. Smith conducted a number of the tests. Principal Technician for all the elastomer tests was Mr. S. Hamil.

TABLE OF CONTENTS

LIST OF FIGURES

LIST OF FIGURES, CONT'D

I. SUMMARY

This report presents the results of a program of analysis and test to determine the dynamic properties of elastomer cartridges operating under a rotating load. These measured properties were compared to predictions based on previous results of uni-directional reciprocating tests with the same elastomer material.

The test method for the dynamic stiffness and damping measurements was essentially the same as the Base Excitation Resonant Mass Method used and reported previously. The primary difference is that the exciting force used for these most recent tests was exerted by rotating unbalance in a rotational test rig rather than by a shake table. The specimens tested were: two rectangular cross-section continuous ring cartridges of different cross-section and three cylindrical button cartridges of different button thickness. Tests were performed for strains from about 0.0001 to about 0.01 (double amplitude), at a temperature of about 26°C. The material tested was a broad temperature range (BTR) polybutadiene.

Material properties and prediction equations determined previously were used to make numerical predictions of stiffness, damping, and loss coefficient for the test elements, with encouraging results. Strain was shown to be an important parameter in determining these dynamic properties, particularly damping and loss coefficient.

II. INTRODUCTION

The use of support damping as a means to control rotating machinery vibrations is seeing increasingly wide application in advanced turbo-machinery. It will also have an important role to play in advanced, flexible, power transmission shafting. Presently, the most common type of damper in these applications is the squeeze-film damper in parallel with some type of mechanical flexure.

Elastomer dampers are an attractive alternative to the squeeze film for rotating machinery and other applications because of their simplicity; their inherent combination of stiffness and damping; their compactness; and their lack of need for seals or oil supply. In the form of O-rings or cartridges they are being considered for low-cost engine applications and for helicopter transmission shafting.

Two of the factors which resist the growth in application of elastomer dampers are the limited availability of design-oriented data on their dynamic behavior and limited quantification of the problems to be encountered in their application. Dynamic testing under controlled conditions, coupled with practical interpretation of the test results, is the means to fill this need. Thereby, the influence of important geometrical, environmental, and chemical design parameters can be determined.

A program for testing and analysis of elastomer materials has been in progress at MTI since 1971. The objectives of the program are to develop elastomer dynamics technology and to reduce the technology to a form in which it can be readily applied in design.

Experimental and analytical methods are employed in meeting these objectives. Firstly, from a limited number of tests, general properties are sought which characterize an elastomer material. Secondly, prediction methods are sought which employ these material properties, in combination with appropriate geometry effects, to yield values for stiffness and damping of particular elastomer configurations.

This report is the fourth in a series. Preceding reports (References 1, 2, and 3) have described the development and refinement of a powerful test technique, the Base Excitation Resonant Mass (BERM) method, and its application

to the development of elastomer element properties in a controlled temperature environment under conditions of low and high dissipation for a variety of geometries. The BERM method most conveniently supplies data in the 100 to 1000 Hz frequency range into which the majority of rotating machinery vibration problems fall. Important features of the method are its controlled temperature environment; its ability to apply controlled high or low levels of dissipation at frequencies up to 1000 Hz or higher; its exploitation of mechanical resonance to achieve phase angles clustered around 90 degrees; and its determination of stiffness and damping from accelerometer signals only, each processed by identical electronics, to minimize spurious phase errors in the data.

The work presented herein provides correlation of analytical predictive procedures developed from previously generated test results (References 1, 2, and 3) under a reciprocating load, with test results currently obtained under a rotating load. The importance of this correlation cannot be stressed too strongly. Under earlier phases of this program (References 1, 2 and 3), it was found that predicting and obtaining dynamic properties for elastomer specimens operating under a reciprocating load was not difficult. However, the ultimate aim of this technology is to provide designer-oriented information for use in the design of elastomer dampers for rotating machinery. Therefore, the predictive methods obtained from reciprocating elastomer tests are useful only if it can be shown that those methods are applicable to an elastomer element which is subjected to a rotating load. To this end a rotating load test rig was designed and built. The requirements for this test rig were quite severe. The test rig had to permit easy exchange of elastomer cartridge specimens; it had to be possible to change the level of exciting force; it had to be possible to implement the Base Excitation Resonant Mass technique to generate test data; and it had to be possible to run the test for several minutes at frequencies up to 1000 Hz. The test rig met these basic requirements and allowed stiffness and damping properties of 5 different elastomer cartridge configurations to be determined under a rotating excitation. At the same time it was found that, superimposed on the desired translatory motion of the test rig resonant mass, was significant conical motion. This conical motion presented difficulties in data reduction as discussed in the body of the report. It also diminished the amplitude and peak resonant frequency of the translatory component which had been predicted

assuming pure translatory motion; thus, additional project goals of imposing up to 5 mils double amplitude and including translatory resonant response at up to 1000 Hz were not met.

The starting point for accumulation of information is testing, and the rotating load test rig provided the source of test data within this phase of this program. The output of the tests was raw data (amplitudes, phase angles, etc.) which was converted by automated data analysis methods to specimen properties - that is, stiffness and damping of the elements being tested.

The following sections of the report present, first, a summary of results, conclusions, and recommendations. Then follows a description of test methods, including parameter ranges, a presentation of the test results, and a discussion of these results.

III. SUMMARY OF RESULTS

Although the elastomer cartridges did not respond in a strictly radial mode, as was intended in the design of the test rig, it was generally possible to identify the radial component of the response, from which values of elastomer stiffness and damping could be calculated. However, a conical resonance of the test rig upper bearing housing occurred at about 320 Hz, and near this frequency, it was not possible to reliably isolate the radial components of vibration.

Predictions of ring cartridge stiffness and damping have been made as a function of frequency (independent of strain), using two different algebraic expressions (from Reference [3]). The simplest of these is based on representation of the cartridges as a series of noninteracting beam and column elements. These two simple methods predicted results which differ by a factor of two, but provide a band within which the great majority of measured values lie.

Predictions of button cartridge stiffness and damping have been made as a function of frequency (independent of strain), using two different algebraic expressions (from reference [3]). One of these expressions is based on the assumption that the individual buttons underwent compression loading only. The other expression is based on the assumption that the individual buttons underwent both compression and shear loading. For one of the button cartridge test specimens, the individual buttons were glued to the inner holder only. In this case, the predictions of stiffness based on compression loading agreed more closely with the test results. For the remaining two button cartridge test specimens, the individual buttons were glued to both the inner and outer holders. In these cases, the predictions of stiffness based on combined compression and shear loading agreed more closely with the test results.

Predictions of loss coefficient and damping for the button cartriges based on the expressions of reference [3] were generally higher than the corresponding measured values. This discrepancy for loss coefficient and damping is attributed to the effects of strain, which was substantially lower for the present tests than for those tests upon which the expressions of reference [3] were based. Extrapolation of available data, for the effects of strain on loss coefficient, to apply to the present conditions, results in much closer agreement between predictions and measurements.

IV. CONCLUSIONS AND RECOMMENDATIONS

On the basis of the results presented in this report, the following conclusions are drawn.

1. The dynamic properties of polybutadiene elastomer cartridges under rotating loading exhibit satisfactory agreement with those obtained under uni-directional reciprocating loading.
2. For low strains, elastomer stiffness is relatively insensitive to change in strain. Stiffness decreases slightly with increases in strain.
3. For low strains, elastomer damping and loss coefficient are very sensitive to changes in strain. Increasing strain results in increases in elastomer damping and loss coefficient.
4. The degree to which shear loading occurs in an elastomer cartridge is dependent on the existence of bonding between the elastomer elements and the specimen holders.
5. To fully define the dynamic behavior of an elastomer, data at both low and high strain levels must be obtained.
6. For design purposes cautious reliance can be placed in predictions of polybutadiene stiffness and corresponding resonant frequencies using the predictive methods discussed herein.
7. Designs based on corresponding polybutadiene damping predictions should, realistically, be tolerant of a factor of two uncertainty in damping and in corresponding amplitudes of response (as they should using state-of-the-art prediction methods for any other damper types).

For future investigations, the following recommendations are made.

1. The understanding of the dynamic behavior of polybutadiene elastomer elements will be improved by obtaining further reciprocating load data at very low strain levels and by relating it to the present test data.
2. Simple methods for including strain dependence of dynamic behavior in elastomer design practice should be developed.

3. Material and geometrical property tests for a number of different elastomer materials should be performed to determine the extent to which the presently discussed predictive methods can be generalized, and to establish a broad data base of elastomer dynamic profiles.

4. Application studies, analytical and experimental, should be performed to determine the benefits and limitations of elastomer elements as vibration control elements.

5. Successful short-term application tests should be followed by tests for life and survivability to determine the extent to which these problems will limit application.

V. EXPERIMENTAL DESIGN AND DESCRIPTION OF TESTS

An Elastomer Cartridge Rotating Load Test Rig was used to test the dynamic properties of the elastomer samples. This test rig employed a forced vibration, resonant mass principle in which rotating unbalance provided the exciting force. The test rig was designed to allow the frequency of resonance to be modified by changing the amount of resonant mass being supported by the elastomer cartridge specimen. Acquisition of data was, however, not limited to the resonance condition of the system. In fact, data obtained at the resonance frequency of each mass-spring combination was just one of several data points acquired at several vibration frequencies around resonance, where significant amplitude ratios between rotor and resonant mass vibration existed. This method of generating test data for calculating dynamic elastomer properties was essentially the same as the Base Excitation Resonant Mass Technique employed in earlier phases of this program, except that in this case the elastomer specimen was being subjected to a rotating load rather than a reciprocating load. The following sections present a description of the test rig, the design of the elastomer test samples, the methods of prediction of elastomer properties, the instrumentation as it was used for the recording of test data, the procedures involved in the testing, and the range of test parameters investigated.

Description of Elastomer Cartridge Rotating Load Test Rig

The Elastomer Cartridge Rotating Test Rig is shown in a sketch in Figure 1 and as a photograph in Figure 2. The components of the test rig are shown in Figure 3. The lower housing of this test rig was securely mounted to a rigid support structure. The upper housing of this test rig was attached to the lower section by flexures which were designed to have a low radial stiffness (1.75×10^5 N/m) and high angular and axial stiffnesses. Therefore, the upper housing was free to translate relative to the lower housing, but its rotation and axial motion were strongly resisted. The rotating shaft was supported in each of these housings by a single angular contact ball bearing. The bearings were preloaded against each other using wave spring washers. The direction of preloading was designed to require the flexures to be statically loaded in tension to eliminate any danger of buckling the flexures. Oil jet lubricaton was used to lubricate and cool the bearings. This test rig was designed to allow it to be used for testing O-rings as well as elastomer cartridges, as shown in the sketch in Figure 1. The elastomer cartridges are described in detail in the next section of this report.

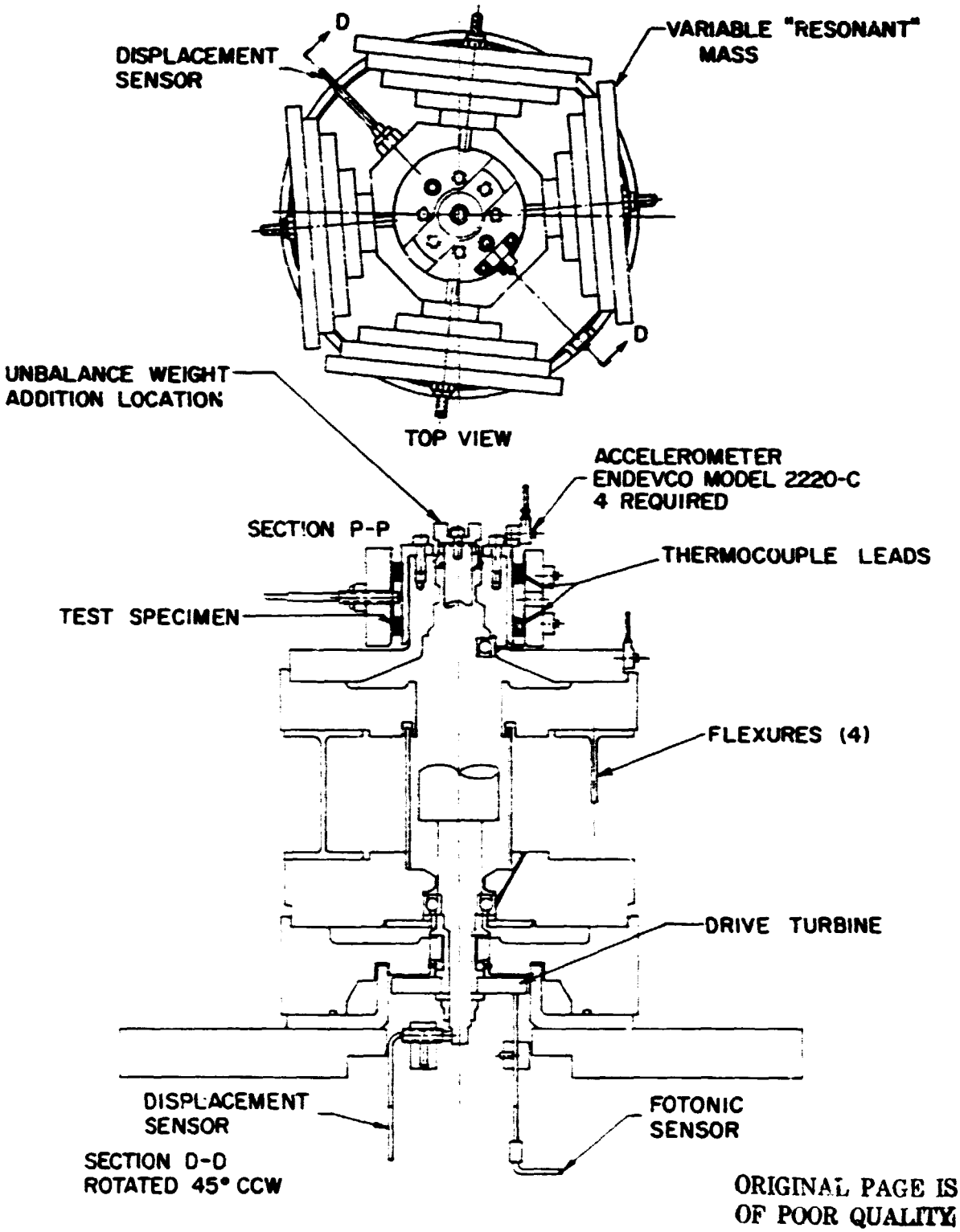

Figure 1. Sketch of Elastomer Cartridge Rotating Load Test Rig

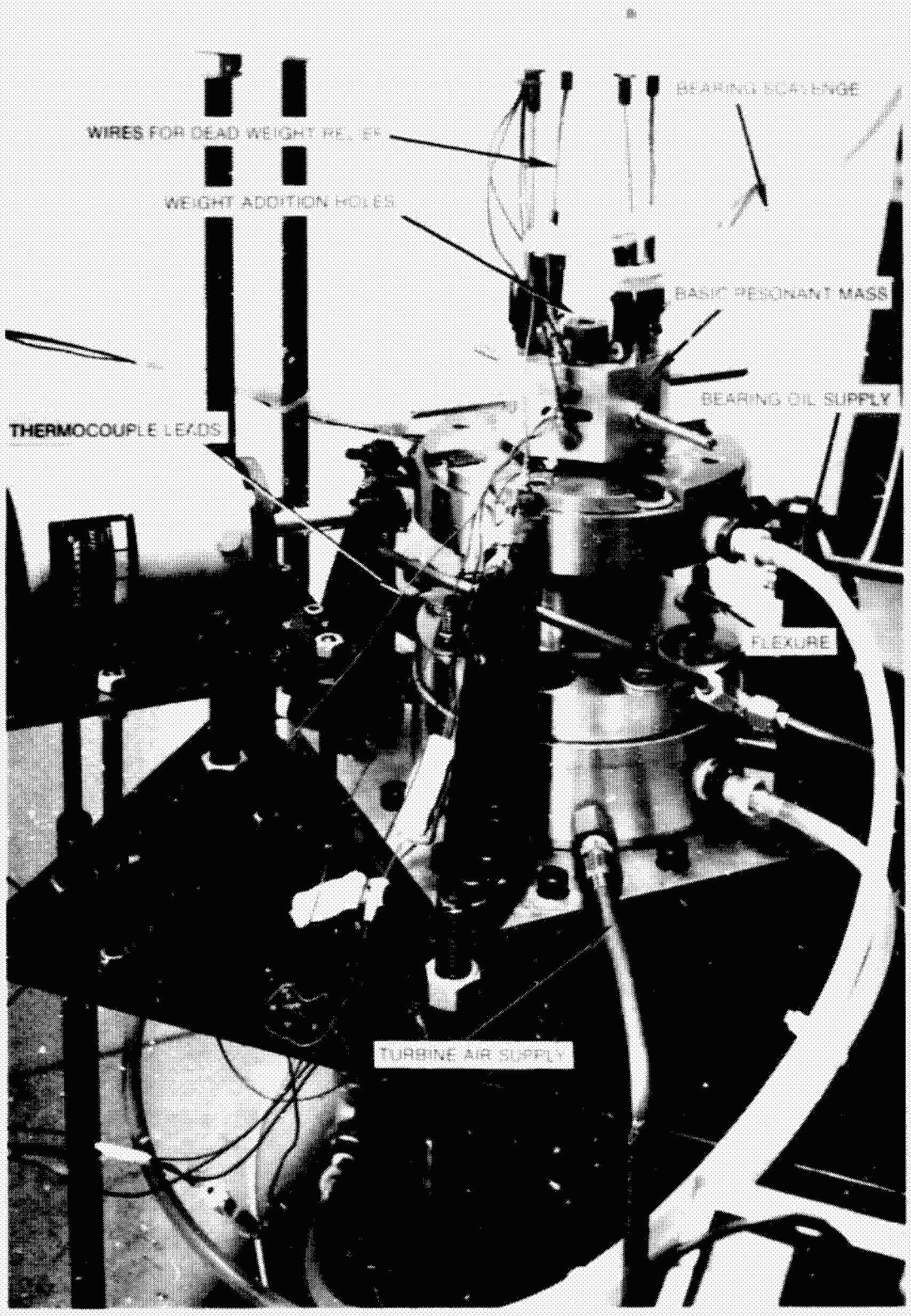

Fig. 2 Elastomer Cartridge Rotating Load Test Rig

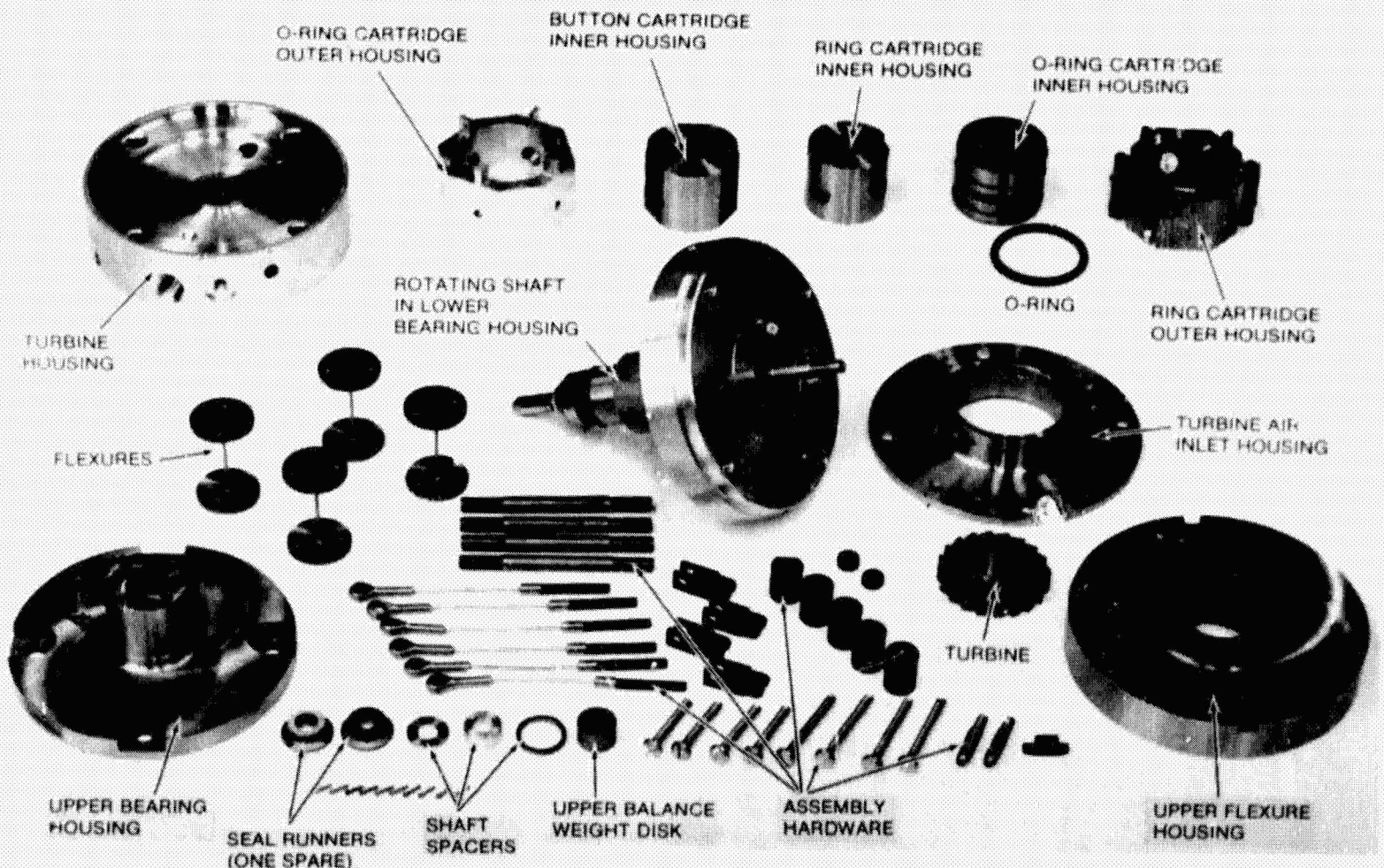

Fig. 3 Components of Rotating Load Test Rig During Assembly

MTI-17706

The test rig shaft had an air turbine drive. The turbine wheel was mounted to the bottom of the shaft with an interference fit to prevent any relative motion between the turbine wheel and the shaft. A series of threaded holes were available in the turbine wheel for adding balance (or unbalance) weights to the bottom of the shaft. A disk was attached to the top of the shaft which also had a series of threaded holes for balance weights. The exciting force for the elastomer response was changed by the addition of weights to the disk at the top of the shaft.

The test rig was instrumented with accelerometers, displacement probes, thermocouples, and a Fotonic Sensor^{R} (fiber optic pickup). This instrumentation is described in detail in a later section of this report.

As an integral part of the test rig design, a series of analytical critical speed and unbalance response predictions were made. Three critical speeds were predicted to occur in or near the operating speed range of the test rig. The predicted mode shapes for these critical speeds are presented in the sketches in Figure 4. Since the flexure stiffness was designed to be at least an order of magnitude less than the elastomer cartridge stiffness, the mode of the lowest test rig resonance involved in-phase motion of the test rig upper bearing housing, elastomer cartridge, and resonant mass on the flexures as illustrated in the sketch in Figure 4a. In this mode, the rotating shaft of the test rig remained rigid. The frequency at which this resonance occurred was a mild function of the resonant mass, since the resonant mass was only part of the dynamic mass in this mode of resonance, ranging from about 13 to 25 Hz, well below the frequency range of interest for the elastomer tests. The second test rig resonance was that used for the elastomer tests. This mode involved the same motion of the test rig upper bearing housing and elastomer cartridge inner housing as the first test rig resonance. However, the elastomer cartridge outer housing and the resonant mass moved out of phase with the inner housing, as illustrated in Figure 4b. The frequency at which this resonance occurred was a function of both resonant mass and the dynamic properties of the elastomer cartridges, ranging from about 200 Hz to 650 Hz. For this resonance, as for the first resonance, the test rig rotating shaft was not expected to bend. The third resonance of the test rig, which was expected to occur above 1000 Hz, involved bending of the test rig rotating shaft between the lower bearing and the turbine. This mode involved little motion of the upper portion of the test rig

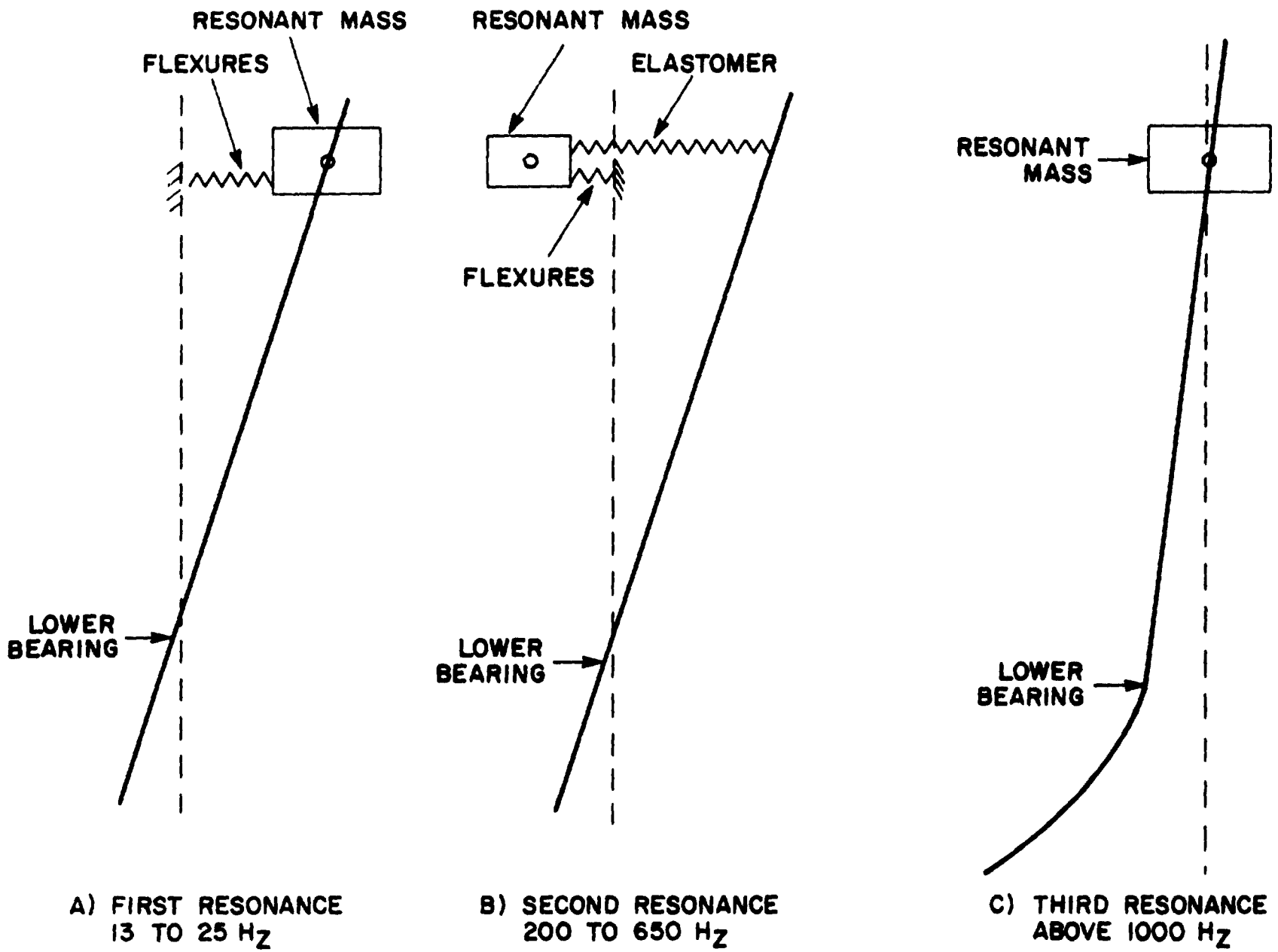

Figure 4. Mode Shapes of Rotating Load Test Rig Resonances

rotating shaft, the upper bearing housing, and the resonant mass. Although this resonance was expected to occur above 1000 Hz, a significant amount of unbalance in the turbine wheel could, and did, begin to excite this mode at frequencies as low as about 800 Hz. However, the response to this mode of resonance was not significant within the frequency range of the elastomer tests.

Description of Elastomer Cartridge Test Samples

Test samples were designed to be used with the Elastomer Cartridge Rotating Test Rig to determine the dynamic stiffness and damping of an elastomer cartridge under rotational radial loading. The selections of test sample material and configurations are discussed below.

Material Selection

The initial selection of polybutadiene as test material had already taken place during an earlier phase of this program reported in Reference 2. Restated briefly, the choice of polybutadiene, which is classed as a Broad Temperature Range (BTR) elastomer, was primarily based upon the desire to test a material that was not overly sensitive to small variations in ambient temperatures nor to the temperature variation induced in the sample through vibration testing.

The choice of polybutadiene among BTR elastomers was based upon the manufacturer's* recommendation founded on manufacturing considerations, such as the achievement of consistent material properties from batch-to-batch. This material, which carries the manufacturer's designation NEX156G, has a nominal hardness of 70 durometers (or Shore A Hardness) and has the highest hardness and damping of those available from the manufacturer.

Test Sample Configurations

Two test sample configurations were tested:

- Ring Cartridge Type Samples
- Button Cartridge Type Samples

*Nichols Engineering, Incorporated, Shelton, Connecticut.

Ring Cartridge Test Samples - Each of these test specimens (shown in a sketch in Figure 5) consisted of two continuous axisymmetric elastometric rings of basically rectangular cross-section. These rings were each held between and cemented to the cylindrical surfaces of two shell structures with a cyanoacrylate glue (Eastman 910 MHP). The outer housings were split to facilitate the assembly of these test elements and to allow a positive radial preload to be applied, so ensuring that the elastomer-metal bonds remain in compression during testing. One of these assembled test elements (shown in the photographs in Figures 6 and 7) could then be mounted on or removed from the test rig as a unit. When assembled to the test fixture, the inner housing of the test element was secured to the upper housing of the test rig, while the elastomer supported outer housing was attached to, and therefore, became part of, the resonant mass.

Sizing studies for the ring cartridge were performed. A minimum value for inner diameter was established from other design considerations, such as bearing size. It was decided to use this minimum value for the inner diameter and to determine the outer diameter by using the same material thickness as was used for the previous cartridge tests, 0.188 inches (0.0048 meters).

Two sets of dimensions were selected for the test configuration and are shown in Table 1. The sizing combines desirable stiffness values with dimensions which fit the available test space yet allow for good rigidity of the holders. Two values of the ratio of length to radial thickness are represented for the same value of diameter. The predicted stiffnesses are discussed in a later section of this report.

TABLE 1

DIMENSIONS OF RING CARTRIDGES

Sample Number	Inner Diameter		Outer Diameter		Length	
	Meters	Inches	Meters	Inches	Meters	Inches
1	0.064	2.50	0.073	2.875	0.0048	0.188
2	0.064	2.50	0.073	2.875	0.0024	0.095

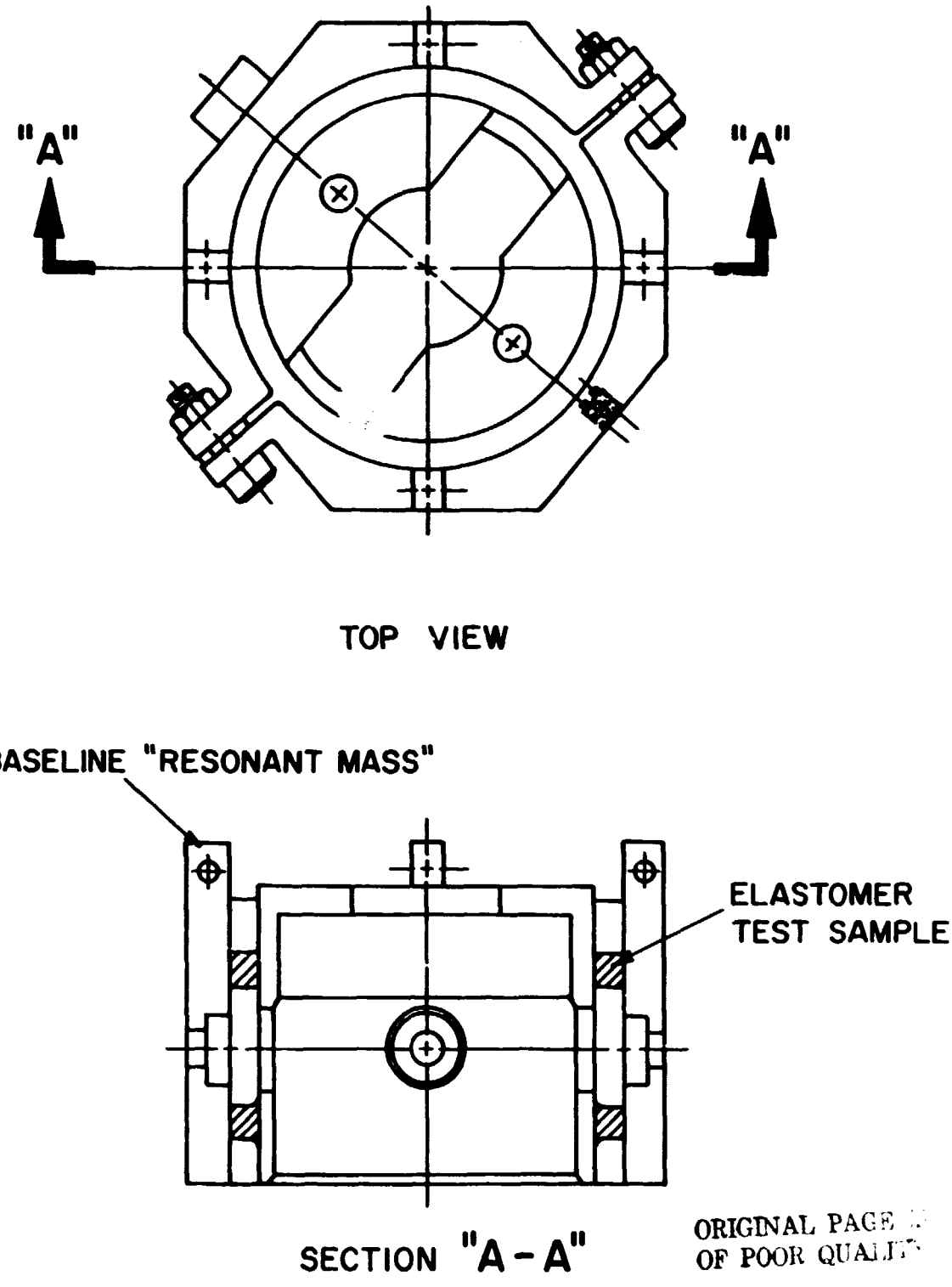

Figure 5. Sketch of Rectangular Cross Section Elastomer Ring Cartridge

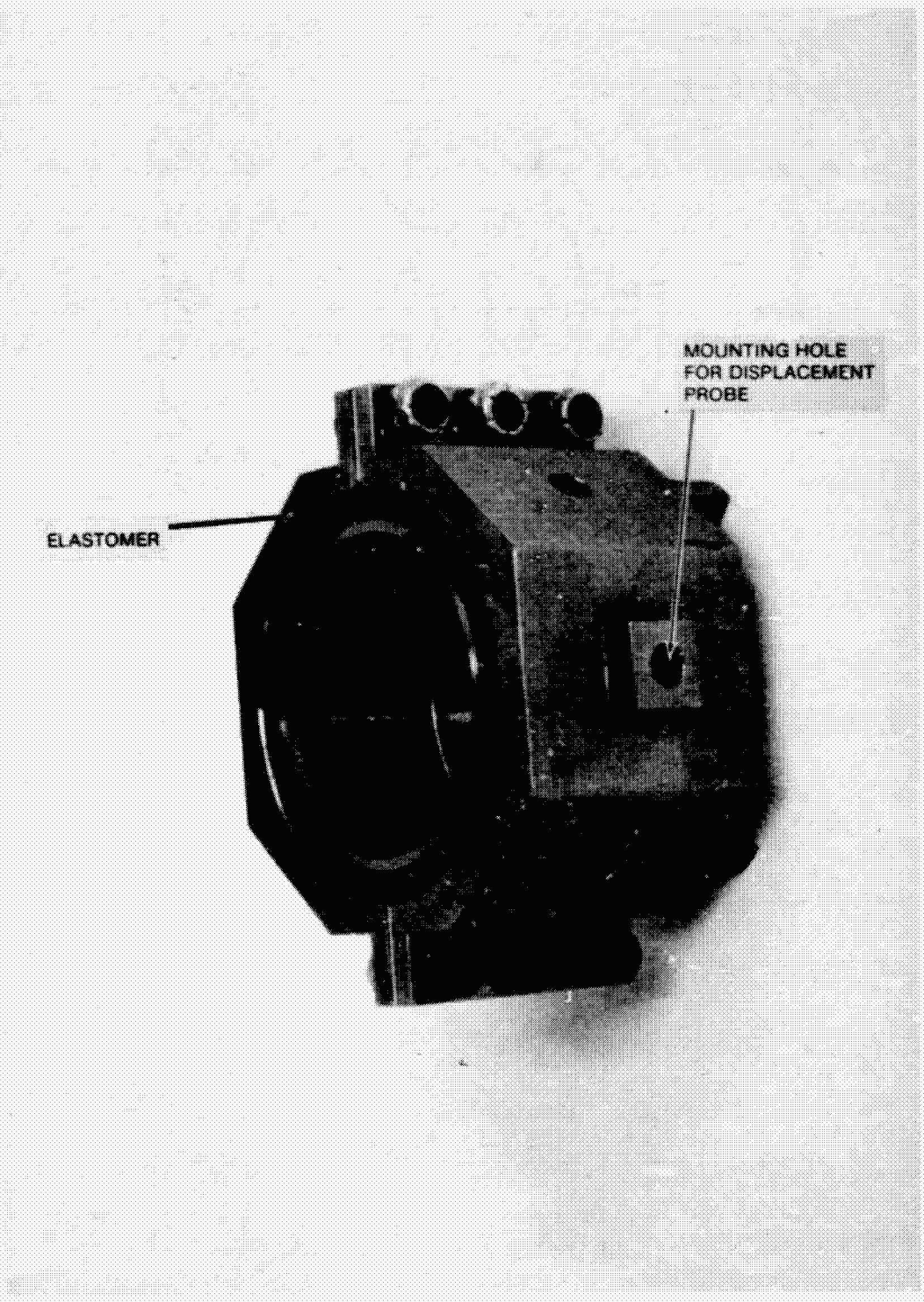

Fig. 6 View of Assembled Continuous Ring Elastomer Cartridge Showing Mounting Hole for Displacement Probe

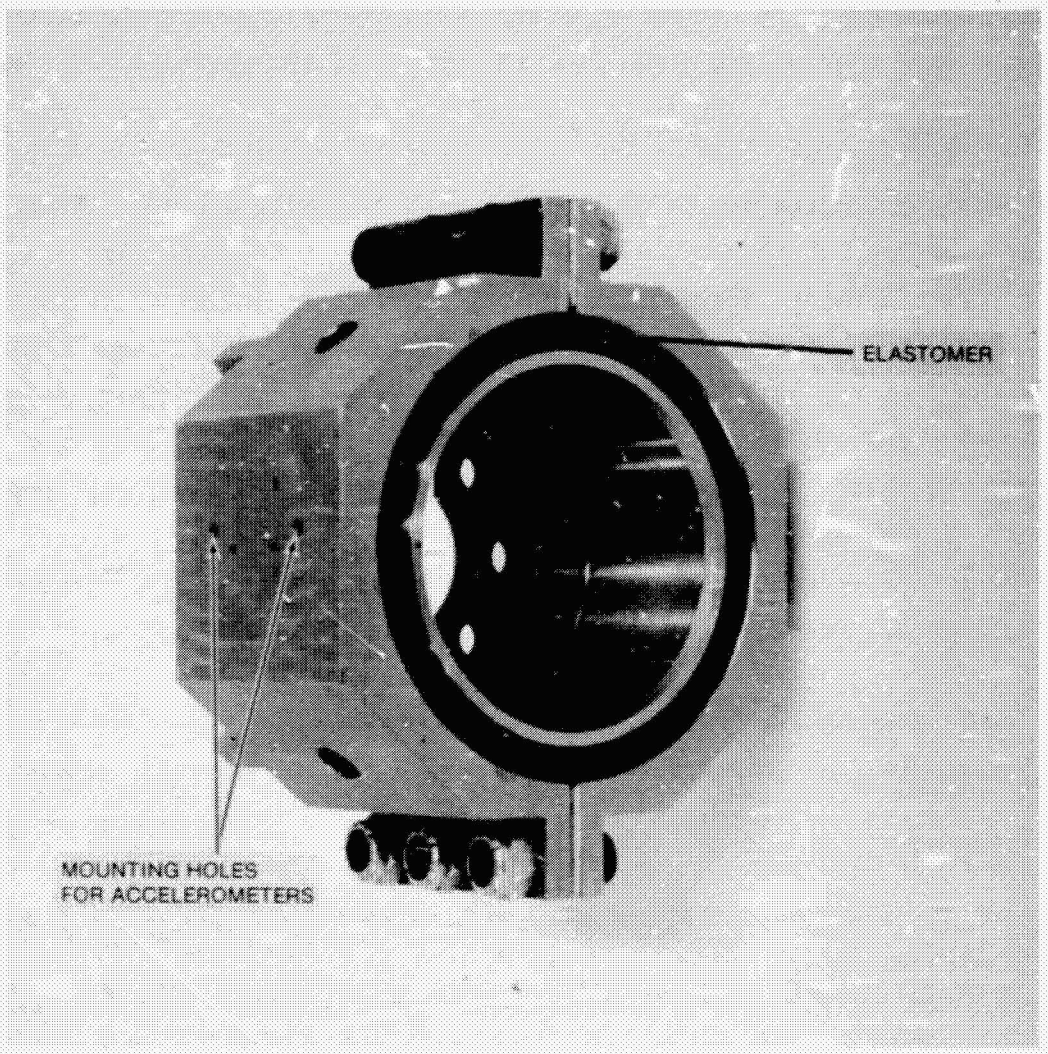

Fig. 7 View of Assembled Continuous Ring Elastomer Cartridge Showing Mounting Holes for Accelerometers

Button Cartridge Test Samples - Each of these test specimens (shown in a sketch in Figure 8) consisted of two rows of cylindrical elastomer compression elements or "buttons" evenly distributed about the origin of the rotating force vector. These buttons were held between the flat surfaces of two shell structures. In all cases, the buttons were cemented to the inner housing with a cyanoacrylate glue and, in all but one case (as explained later in this report), the buttons were also cemented to the outer housing with the same glue. The buttons were located such that a line drawn from the origin of the rotating force vector through the center of any of the buttons would form a right angle with either face of that button. One of the inner housings with the buttons attached is shown in the photographs in Figures 9 and 10. As with the ring cartridges, the outer housings for the button cartridges were split to facilitate the assembly of the test elements and to allow a positive radial preload to be applied. Therefore, each of these test elements could also be mounted on or removed from the test rig as a unit. In this way, both the ring and button cartridges could be pre-assembled and then quickly substituted on the test rig when desired during the test program. When assembled to the test fixture, the inner housing of one of the button cartridge test elements was secured to the upper housing of the test rig, while the elastomer supported outer housing was attached to, and, therefore, became part of the resonant mass.

For each of the button cartridges, each row of compression elements consisted of three 0.50 inch (0.0127 meters) diameter cylinders spaced circumferentially equidistant on a 2.50 inch (0.0635 meter) diameter. The diameter dimension was chosen to be 0.50 inch, since polybutadiene rod of this diameter was readily available. Three thickness (height) dimensions were selected for the test configuration and are shown in Table 2.

Besides material availability, the button cartridge afforded two additional advantages. Firstly, no special molding was required; the buttons were simply cut to size, assembled in compression between the two rings, and bonded in place. Secondly, wide controllability of stiffness and damping properties are available by control of the individual button dimensions.

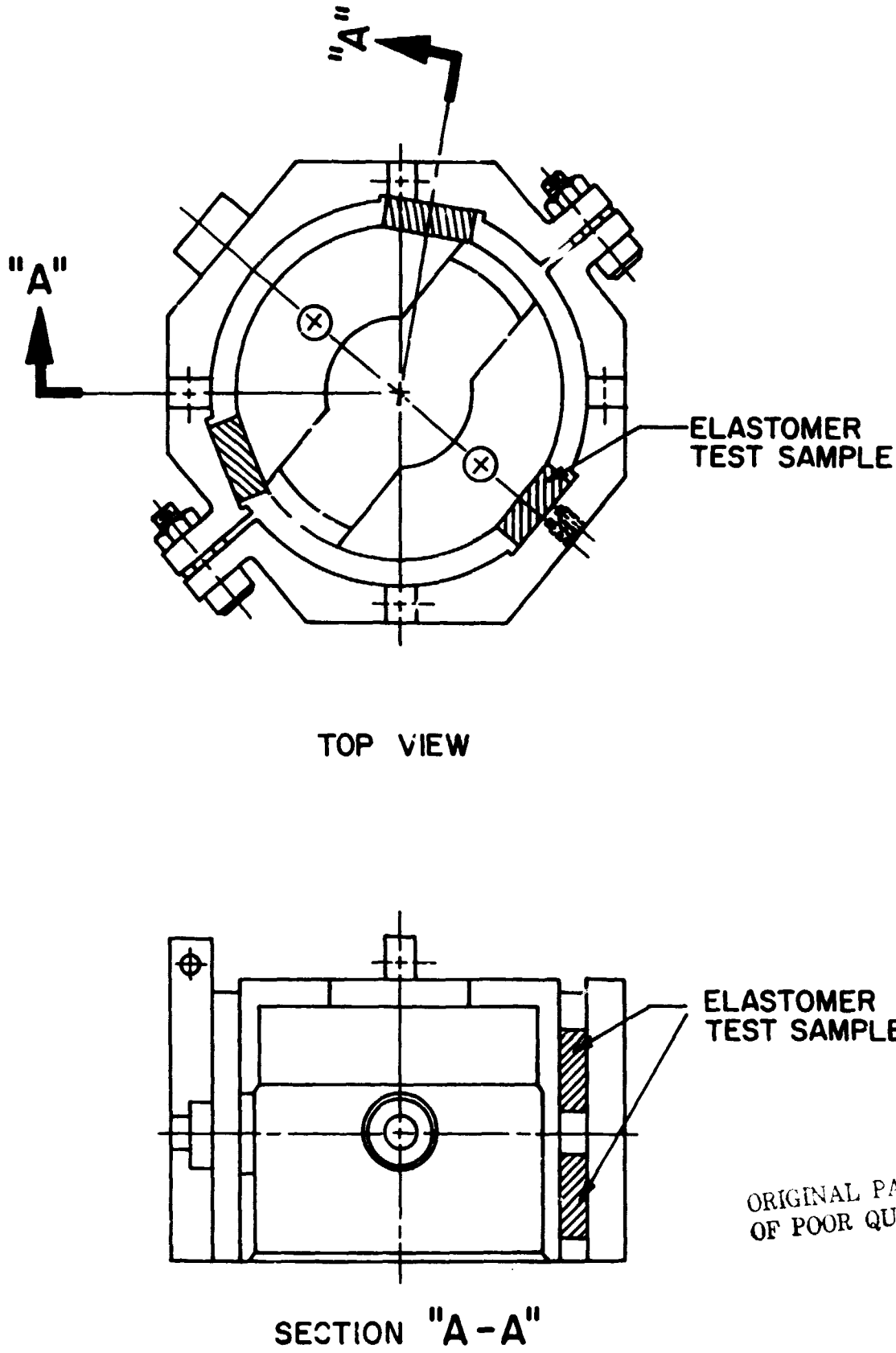

Figure 8. Sketch of Cylindrical Elastomer Button Cartridge

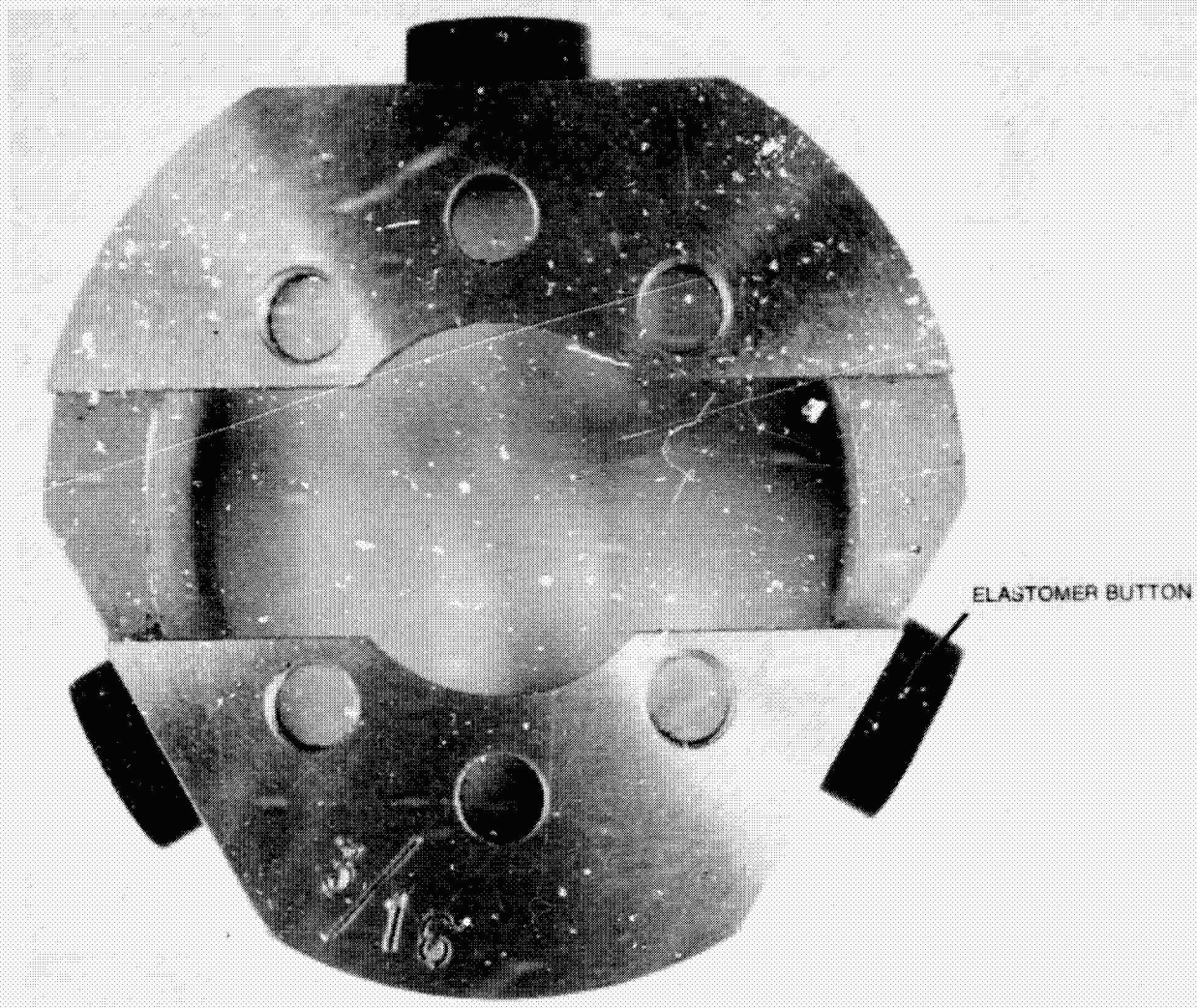

9 Top View of Partially Assembled Cylindrical Button Elastomer Cartridge

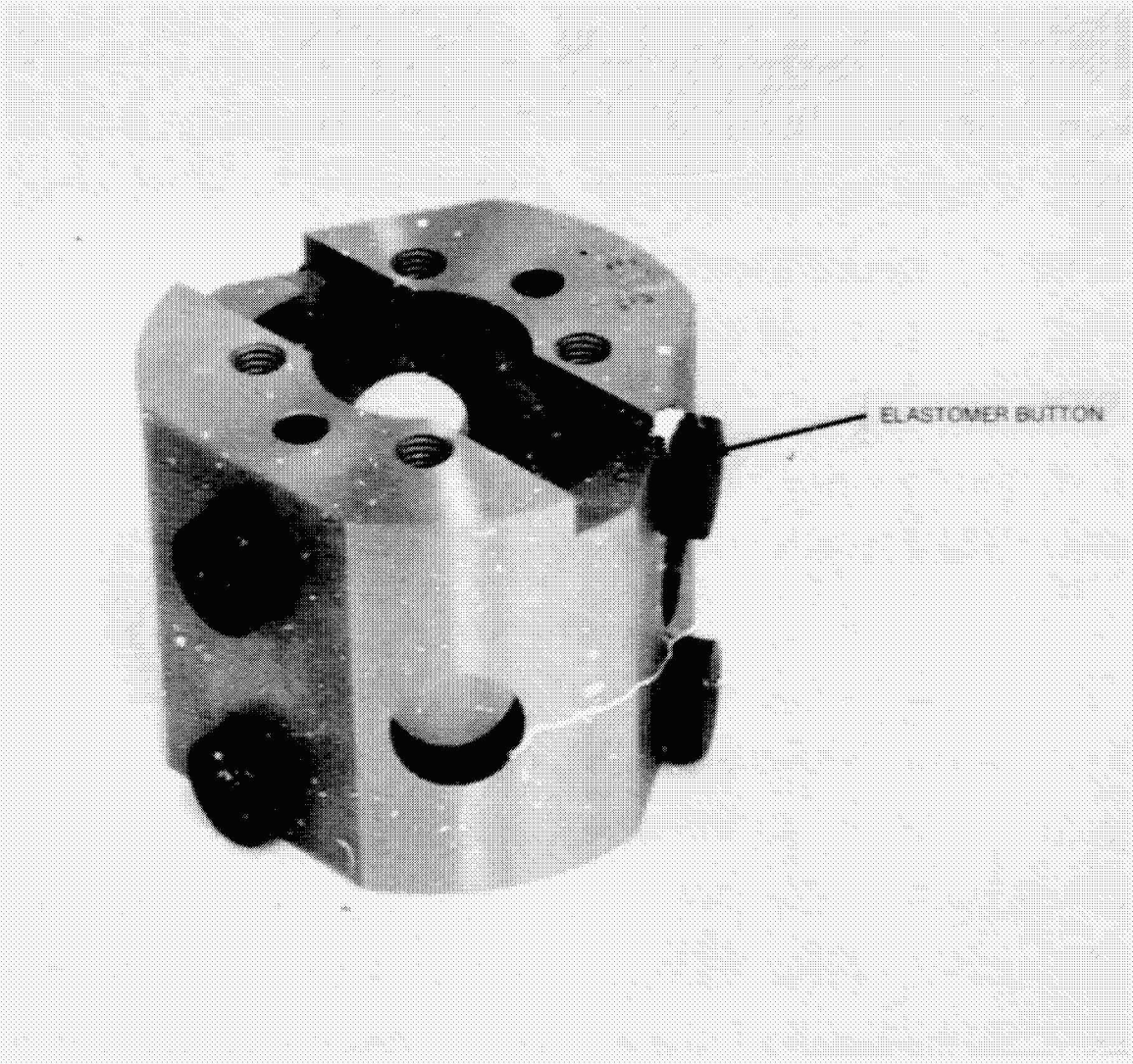

Fig. 10 Side View of Partially Assembled Cylindrical Button Elastomer Cartridge

TABLE 2

DIMENSIONS OF "BUTTON" CARTRIDGES

Sample Number	Inner Diameter		Outer Diameter		Cylinder Diameter		Button Height	
	Meters	Inches	Meters	Inches	Meters	Inches	Meters	Inches
1	0.0635	2.50	0.0699	2.75	0.0127	0.50	.00318	.125
2	0.0635	2.50	0.0683	2.688	0.0127	0.50	.00238	.0938
3	0.0635	2.50	0.0730	2.875	0.0127	0.50	.00476	.188

VI. PREDICTIONS OF DYNAMIC PROPERTIES OF ELASTOMER CARTRIDGE TEST SAMPLES

For the specific geometries, established in the previous section, for the elastomer cartridges to be tested, predictions were made of stiffness and damping based on the conclusions from Reference [3]. The properties for the ring cartridges were predicted as the arithmetic average of the values obtained from equations (1) and (2):

$$K^* = 4\pi G^* NL/\ln(r_2/r_1) \quad (1)$$

$$K^* = 7.5\pi G^* NL/\ln(r_2/r_1)f_1 \quad (2)$$

where,

K^* = complex impedence of ring cartridge $(= K_1 + iK_2)$ N/m

G^* = complex shear modulus of elastomer material $(= G' + iG'')$ N/m

N = number of elastomer elements (rings) in cartridge

L = length of one element (ring)

r_2 = outside radius of one element (ring)

r_1 = inside radius of one element (ring)

$f_1 = 1 + 0.0097L^3/(r_2 - r_1)^3$

K_1 = stiffness N/m

K_2 = damping N/m

G' = storage shear modulus (N/m^2)

G'' = loss shear modulus (N/m^2)

Equation (1) is the Beam-Column formula (with radius effects), as reported in reference [3]. Equation (2) is the Göbel formula (originally from reference [4]), also reported in reference [3]. It was found in reference [3] that the predictions from these two formulae generally bracketed the ring cartridge test results and that an average of the two predictions usually presented a reasonably good estimate of the actual dynamic properties of the ring cartridge of interest. Therefore, it was decided to use this average for predicting the dynamic properties of the ring cartridges to be used for the rotating load tests.

The loading of the individual buttons in the button cartridges was principally compressive. In two of the three button cartridges, the buttons were glued to both the inner and outer housings. In these cases, the buttons would experience shear loading as well. In the third button cartridge (referred to as Button Cartridge #3), the buttons were glued to the inner housing only. It is less likely that these buttons were subjected to any shear loading. However, for all three of the button cartridges, predictions of dynamic properties were conducted, both including and neglecting the effect of shear loading on the buttons, for comparison purposes.

Each of the button cartridges had six elastomer buttons arranged in two rows, with three buttons equally spaced circumferentially in each row. The arrangement and loading of the buttons in one of these rows is illustrated in the sketch in Figure 11. A force F is exerted on the center of the inner housing of the cartridge. The resulting displacement at this point is δ. The corresponding compressive displacement across button #1 is δ, while the corresponding compressive displacement across buttons #2 and #3 is δ times the cosine of sixty degrees, or $\delta/2$. Therefore, assuming all three buttons have an equal compressive stiffness of K_c, the resulting compressive force in button #1 is $K_c\delta$, while the resulting compressive force in each of buttons #2 and #3 is $K_c\delta/2$. There is no shear displacement across button #1, while the shear displacement across buttons #2 and #3 is δ times the sine of sixty degrees, or $\delta\sqrt{3}/2$. The resulting shear force in each of buttons #2 and #3 is $K_s\delta\sqrt{3}/2$, where the buttons have equal shear stiffnesses of K_s. Summing the forces in the x and y directions gives:

$$\Sigma F_x = F = K_c\delta + K_c\delta/2 \cos 60^\circ + K_c\delta/2 \cos 60^\circ + K_s\delta\sqrt{3}/2 \sin 60^\circ + K_s\delta\sqrt{3}/2 \sin 60^\circ = 3/2\,(K_c + K_s)\,\delta$$

$$\Sigma F_y = 0 = K_c\delta/2 \sin 60^\circ - K_c\delta/2 \sin 60^\circ + K_s\delta\sqrt{3}/2 \cos 60^\circ - K_s\delta\sqrt{3}/2 \cos 60^\circ = 0$$

Therefore, the compressive and shear stiffnesses of a ring of three buttons are both equal to three halves of the corresponding stiffnesses of a single button. The same result will be obtained regardless of the direction in which the loading force is taken in the above derivation. The dynamic properties for

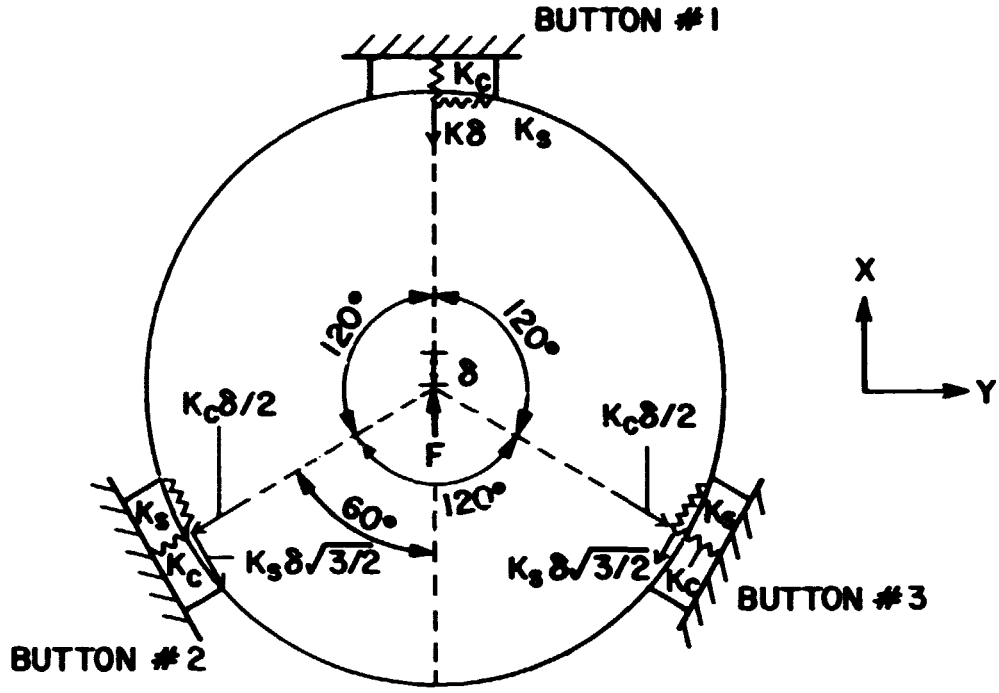

Figure 11. Arrangement and Loading of a Typical Row of Button in a Button Cartridge

the button cartridges were calculated from equations (3) through (6) using an appropriate value for N' (effective number of buttons). Since a single ring of three buttons could be represented by one and one-half buttons, a button cartridge with two such rings could be represented by letting N' be equal to three. Equations (3) and (4) include shear effects and equations (5) and (6) neglect shear effects.

Including Shear:

$$K_1 = 3G' \frac{N'\pi D^2}{4h} \left[1 + \beta' \frac{(D)^2}{(4h)^2}\right] + G' \frac{N'\pi D^2}{4h} \qquad (3)$$

$$K_2 = 3G'' \frac{N'\pi D^2}{4h} \left[1 + \beta'' \frac{(D)^2}{(4h)^2}\right] + G'' \frac{N'\pi D^2}{4h} \qquad (4)$$

Neglecting Shear:

$$K_1 = 3G' \frac{N'\pi D^2}{4h} \left[1 + \beta' \frac{(D)^2}{(4h)^2}\right] \qquad (5)$$

$$K_2 = 3G'' \frac{N'\pi D^2}{4h} \left[1 + \beta'' \frac{(D)^2}{(4h)^2}\right] \qquad (6)$$

where, K_1 = stiffness of button cartridge

K_2 = damping of button cartridge (where $K^* = K_1 + iK_2$)

G' = storage shear modulus of elastomer material

G'' = loss shear modulus of elastomer material (where $G^* = G' + iG''$)

N' = effective number of elastomer elements (buttons) in cartridge

D = diameter of one element (button)

h = thickness of one element (button)

β' = shape factor for stiffness

β'' = shape factor for damping

K_1 is the real part and K_2 is the imaginary part of the complex impedence K^*. G' is the real part and G'' is the imaginary part of the complex shear modulus G^*.

Values for G', G", G* (where G* = G' + iG"), β', and β" were required to make predictions of dynamic stiffness and damping of the elastomer cartridges, based on equations (1) through (6). These values and the means by which they were determined were discussed in reference [3]. Briefly, these values were determined from experimental results, as a function of frequency (and temperature), using the same elastomer material (polybutadiene) as was used for the tests reported herein. The values for G', G", and G* were determined from the results of shear specimen tests conducted over a frequency range from 100 to 1000 Hz, for a constant energy dissipation rate. The values for β' and β" were empirically determined from the results of similarly conducted cylindrical compression specimen tests. The following empirical relationships were established for these values, as a function of frequency, for testing at 32 degrees Centigrade:

$$G'(\omega) = 5.686 \times 10^6\ \omega^{0.2037}\ N/m^2$$

$$G''(\omega) = 8.333 \times 10^6\ \omega^{-0.1277}\ N/m^2$$

$$\beta'(\omega) = 12.33\ \omega^{-0.290}\ \text{(dimensionless)}$$

$$\beta''(\omega) = 1.726\ \omega^{0.0299}\ \text{(dimensionless)}$$

where ω is frequency in radians per second. It is noteworthy, based on test results from reference [3], that elastomer component properties are actually sensitive to strain as well as frequency; increasing strain generally results in a slight decrease in dynamic stiffness and a more pronounced increase in dynamic damping (up to a point, beyond which the damping begins to decrease). The level of strain generally encountered in the tests reported herein was somewhat lower than that encountered in the tests from which G' and G" were determined, as reported in reference [3]. Therefore, some discrepancy between predictions and test results for the current tests, particularly as related to damping values, was to be expected; as will be shown, such discrepancies were encountered for damping and were consistent with the effects of strain discussed here.

The elastomer dynamic property predictions, based on equations (1) through (6) for 500 Hz, are presented for the ring cartridges in Table 3 and for the button cartridges in Table 4. In addition to these predictions, because of the

TABLE 3

PREDICTIONS OF STIFFNESS AND DAMPING AT 500Hz FOR RING CARTRIDGES

Sample Number	Stiffness of Cartridge N/M	Stiffness of Cartridge LB/IN.	Damping of Cartridge N/M	Damping of Cartridge LB/IN.
1	2.0×10^7	1.1×10^5	3.3×10^6	1.9×10^4
2	1.0×10^7	5.7×10^4	1.6×10^6	9.3×10^3

TABLE 4

PREDICTIONS OF STIFFNESS AND DAMPING AT 500Hz FOR BUTTON CARTRIDGES

Sample Number	Stiffness of Cartridge N/M	Stiffness of Cartridge LB/IN.	Damping of Cartridge N/M	Damping of Cartridge LB/IN.
1 (with shear)	1.7×10^7	9.7×10^4	3.8×10^6	2.2×10^4
2 (with shear)	3.1×10^7	1.8×10^5	7.5×10^6	4.3×10^4
3 (with shear)	8.4×10^6	4.8×10^4	1.6×10^6	9.1×10^3
3 (without shear)	6.9×10^6	3.9×10^4	1.4×10^6	8.0×10^3

difference in strain level discussed above, the test results for loss coefficient (ratio of damping to stiffness) were compared to values extrapolated from Figure 12 (reproduced from reference [3]), which indicates the effect of strain on loss coefficient for various geometries.

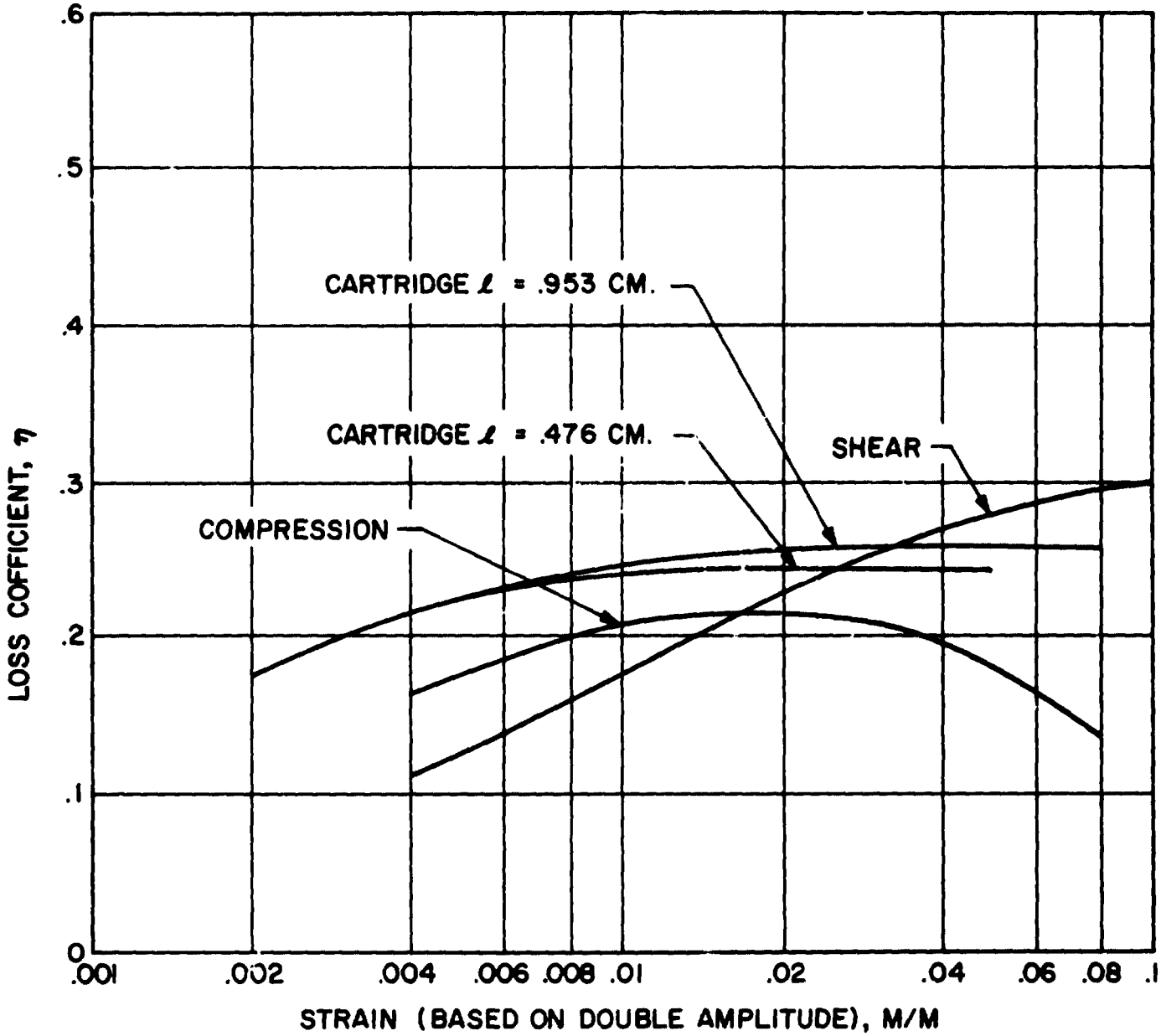

Figure 12. Loss Coefficient as a Function of Strain and Elastomer Specimen (from Reference 3)

VII. INSTRUMENTATION

The uncomplicated measurement requirements of the base excitation resonant mass testing method have been expounded before (see reference [1]). The test method for the rotating load test rig was essentially the same, with the major difference being that the excitation was provided by a rotating unbalance force rather than by a uni-directional shake table. Stated briefly, the measurement requirements for the experimental investigation involving the rotating load test rig were as follows:

1. Acceleration measurement of the elastomer inner support housing attached to the upper bearing housing
2. Acceleration measurement of the elastomer outer support housing attached to the resonant mass
3. Phase angle measurement between acceleration measurements (1) and (2) above
4. Displacement measurement between the two elastomer support housings (relative amplitude across the elastomer)
5. Vibration frequency
6. Temperature of elastomer support housings and bearing housings (for reference only).

The input acceleration (1) was determined from two accelerometers located on the upper bearing housing of the test rig. Output acceleration on the resonant mass (2) was determined from two accelerometers mounted directly to the elastomer outer support housing. The use of two input and two output accelerometers, aligned radially and separated axially, with their output signals displayed on one oscilloscope screen, permitted immediate detection of any angular motion of either of the elastomer support housings. When angular motions occur, they manifest themselves either as amplitude or phase angle differences between the two input accelerometers or the two output accelerometers, or as a combination of both amplitude and phase angle variations (further discussion of angular motion can be found in the next section of this report). To facilitate the comparison of these accelerations, the outputs of the four accelerometers were simultaneously displayed on a four channel oscilloscope. In order to clarify the oscilloscope display of the input accelerometer signals, 2 KHz low-pass filters were used to remove the high frequency noise originating in the rolling-element

bearings. The displacement measurement (4) between the two elastomer support housings (relative amplitude across the elastomer) was accomplished with a noncontacting eddy current type sensor.

Chromel-alumel type thermocouples were used to measure the temperature in the metal of both elastomer support housings directly adjacent to the elastomer specimens (four thermocouples in all). Similar thermocouples were also used to measure the temperature in the metal of both bearing housings directly adjacent to the outer races of the test rig bearings. The bearing thermocouple outputs were monitored in order to ensure that the bearings did not overheat. During the course of the tests, overheating of the bearings never occurred. The elastomer thermocouple outputs were monitored in order to estimate the extent of self-heating that was occurring in the elastomer elements. The elastomer thermocouples never indicated an increase in temperature of more than five degrees Centigrade. Since the elastomer inner housing generally increased in temperature more than the elastomer outer housing, it was apparent that at least a portion of this temperature rise was due to heat generated in the bearings being dissipated through the elastomer inner support housing. Therefore, it can be assumed that any self-heating of the elastomer elements was minimal.

Displacement and acceleration data were displayed on oscilloscopes in real-time form and were, together with temperatures from individual thermocouples, displayed in digital form for monitoring purposes. Amplitude signals, from the four accelerometers and one displacement sensor (plus an additional displacement sensor located at the bottom end of the test rig shaft and additional accelerometers as described under "Operation of the Test Rig"), were sequentially switched by a minicomputer controlled analog scanner into a two-channel tracking filter, which provided visual readout of vibration frequency and two filtered amplitude signals. One of the input accelerometer signals was fed at all times into one of the two channels of the tracking filter and from there into a phase meter where it served as a reference signal for the measurement of the phase angle of the output acceleration signals and the displacement signal. The d-c values proportional to phase angle and amplitude from the phase meter and tracking filter were then converted into digital form in digital voltmeters and read automatically by a PDP 11/34 minicomputer. The minicomputer acquired the data, performed some specified calculations, and printed the data and the

results of the calculations (including values for stiffness and damping) on a computer terminal used by the test rig operator. A schematic of the data acquisition system is presented in Figure 13.

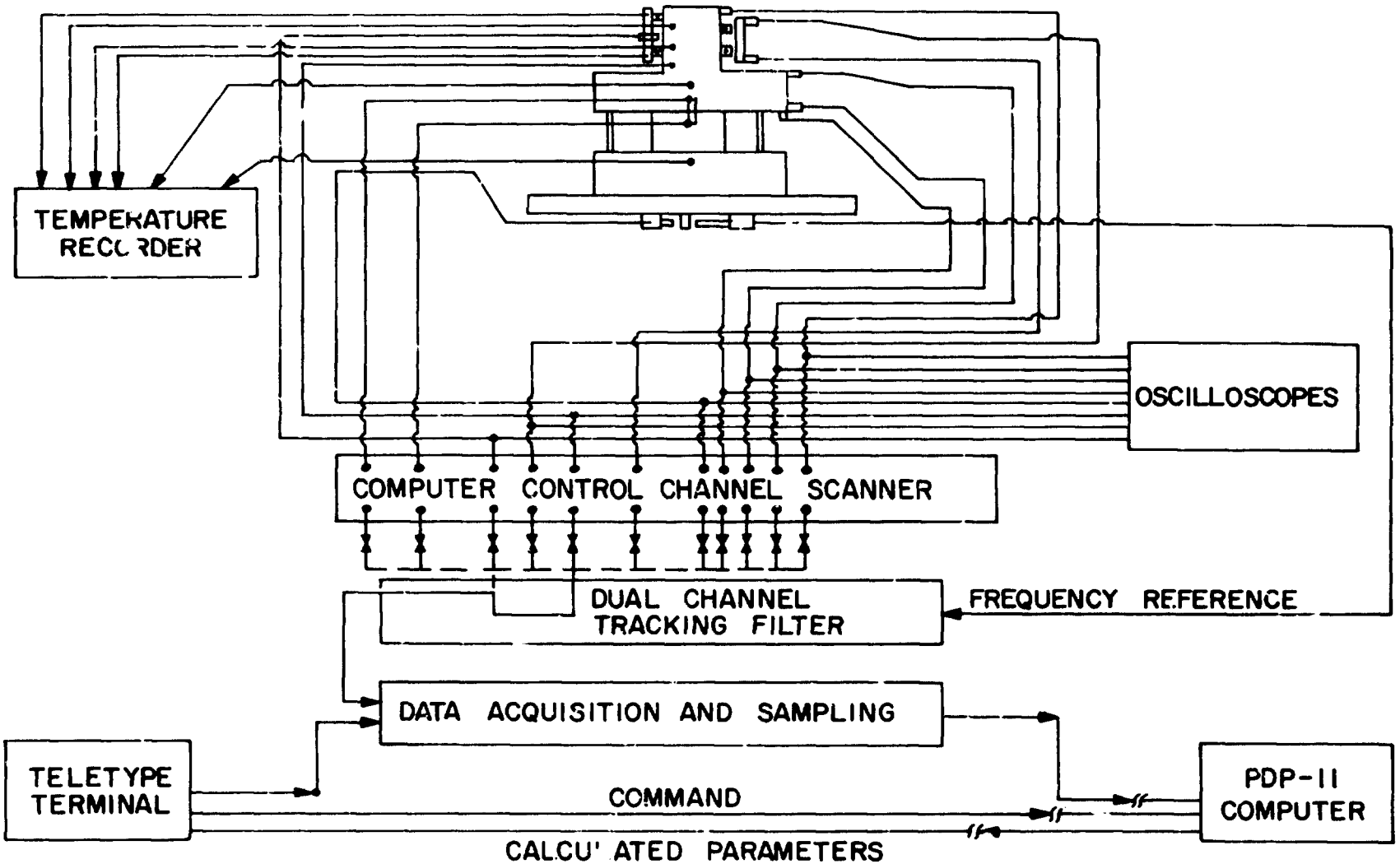

Figure 13. Data Acquisition Schematic

VIII. OPERATION OF THE TEST RIG

The rotating load test rig was assembled and run successfully to over 54,000 rpm (900 Hz), following the resolution of a few minor assembly problems (e.g., seal fits, etc.). The test rig was then balanced, in situ, at about 1200 rpm in order to minimize the response of the first test rig resonance. This balancing was accomplished using data from the displacement probe which was observing the motion at the bottom of the rotating shaft, and by applying the correction weight to the balance weight disk located at the top of the rotating shaft. The amplitude at this resonance was reduced to the point where this resonance could be easily negotiated.

Some additional problems were encountered in evaluating the data obtained from the test rig. First, the initial data acquisition scheme did not produce consistent data because of the large speed fluctuations of the test rig, which was turbine driven and lightly loaded. These fluctuations resulted in speed variations of several hundred rpm over a series of data points. To overcome this problem, an active data acquisition scheme was implemented that would acquire data only within a specified, narrow frequency range. Second, it was found that significant conical motion of the resonant mass was superimposed upon its translatory motion, so complicating the intepretation of the accelerometer data.

Several additional accelerometers were added to the upper bearing housing of the test rig in various locations and orientations in order to aid in identifying the modes of dynamic response of the test rig. These accelerometers revealed that the flexures were not maintaining a purely translatory motion of the upper test rig housing. Instead, they permitted a certain amount of conical excitation to be superimposed on the translatory excitation. In addition, this angular flexibility of the flexures has been found to contribute to a resonance at about 20,000 rpm (referred to as the upper housing support flexure resonance).

To handle the problem of these combined motions, a data reduction scheme was developed to identify the translatory elastomer resonance mode and to derive meaningful values of stiffness and damping from the test data. The analysis

underlying this data reduction scheme is presented in the following section of this report.

Testing Procedures

One of the major features of the current test program was the performance of the scheduled tests at near-resonance conditions. Since phase angle between inner housing excitation and resonant mass response is an accurate indicator of the amount of damping in the region of resonance, measurements should preferably be made in the phase angle range between approximately 15 and 165 degrees (as discussed in reference [2]). (During the tests, this phase angle information from the rotating load test rig was actually read out as negative angles because of the sign convention of the instrumentation setup.) This phase angle range requires that the test frequency be approximately 0.8 to 1.3 times the critical frequency of the elastomer-resonant mass system. Coverage of a broad test frequency range with sufficient test points, therefore, necessitates changes in the size of the resonant mass. The smallest mass consisted of the elastomer test sample outer housing only, with no additional weight attached. Increasingly larger mass combinations were obtained by attaching weights of up to 12 kg directly to the elastomer outer housing.

Once any one of the elastomer test samples had been mounted on the rotating load test rig and the necessary instrumentation was installed and connected, a typical test sequency proceeded as follows:

1. A resonant mass was selected and installed.
2. The rotating load test rig was run and frequency scans were conducted until the approximate resonant frequency of the system was found. (For selected cases, an exact determination of the system resonant frequency was subsequently made by tracing, on an X-Y plotter, d-c value proportional to the resonant mass acceleration amplitude as a function of the rotational frequency.) It may be noted here that, for a rotationally excited single-degree of freedom spring-damper-mass system, resonance occurs at an angle smaller than 90 degrees. The deviation from 90 degrees is essentially determined by the amount of damping in the system.

3. The vibration frequency was reduced to about half of the resonant frequency and data was taken at ascending frequencies until the phase angle increased to a value between 15 and 25 degrees (negative), and a data point was taken with the minicomputer. One data point consisted of one complete set of all amplitudes, associated phase angles, and test frequency. The minicomputer then performed the calculations discussed below and the results were printed on the test operator's console (computer terminal).

4. Stepwise increases in vibration frequency were imposed and several data points were recorded until the phase angle reached approximately 165 degrees (negative).

5. Tests, comprising Steps 1 through 4, were then repeated with each of the remaining masses in turn, each mass giving a dynamic system with a different resonant frequency. A single such test (Steps 1 through 4) required less than an hour to perform.

6. For some of the test specimens, Steps 2 through 4 were repeated for two additional levels of excitation (by changing rotating unbalance) for a single value of resonant mass.

The test results produced by the minicomputer consisted of a printed data set defining the measured amplitudes for each vibration sensor at each frequency point for a series of test cases. The minicomputer also performed all averaging functions and calculations necessary to compute stiffness, K_1, and damping, K_2, for each data point. Since the dynamic motion of the elastomer cartridges was a combination of translatory and conical, it was necessary for the minicomputer to first calculate the transmissibility and phase angle of the translatory motion. A sketch of the accelerometer arrangement for the elastomer cartridge specimens is presented in Figure 14. Assuming that the elastomer cartridges behaved symmetrically and that the center of mass of the outer housing was located midway between the elastomer elements, the translatory motion of the inner and outer elastomer support housings is calculated from equations (7) and (8).

$$A_{IT} = \frac{\ell_4 A_3 + \ell_3 A_4}{\ell_3 + \ell_4} \tag{7}$$

$$A_{OT} = \frac{\ell_2 A_1 + \ell_1 A_2}{\ell_1 + \ell_2} \tag{8}$$

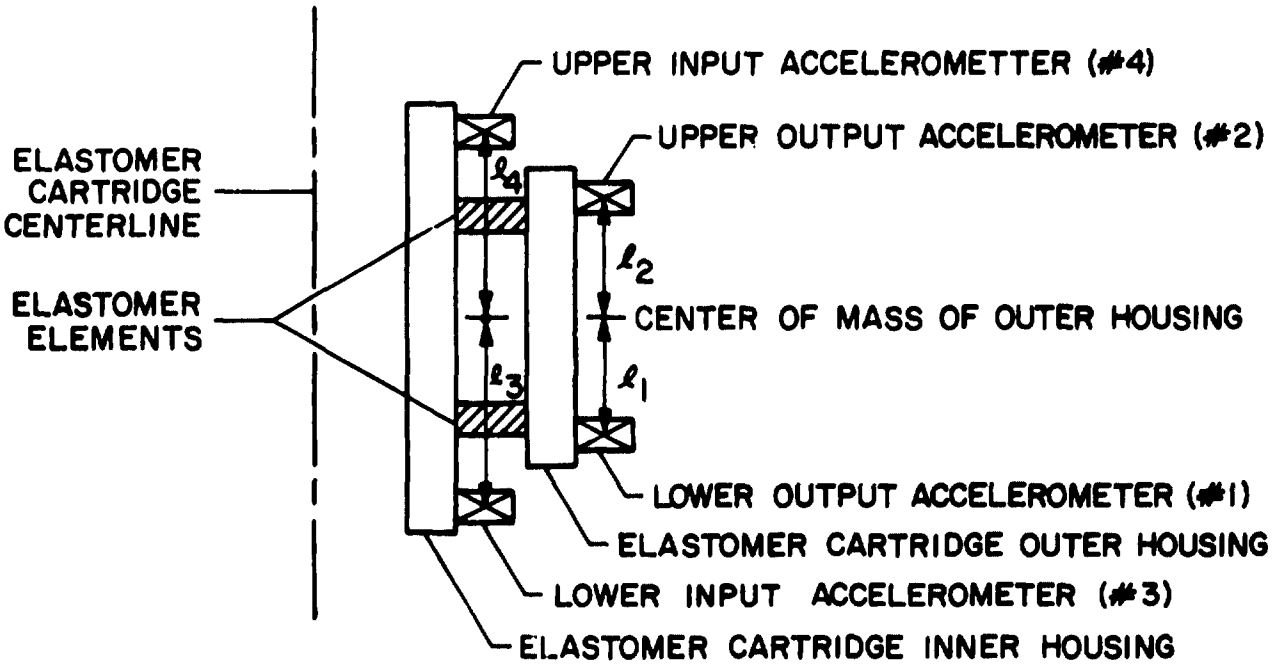

Figure 14. Schematic Diagram of Accelerometer Locations on Elastomer Cartridge Specimens

where,

A_{IT} = translatory acceleration of elastomer inner housing

A_{OT} = translatory acceleration of elastomer outer housing

A_1 = acceleration of lower output accelerometer

A_2 = acceleration of upper output accelerometer

A_3 = acceleration of lower input accelerometer

A_4 = acceleration of upper input accelerometer

ℓ_1 = distance from lower output accelerometer to center of mass of outer housing

ℓ_2 = distance from upper output accelerometer to center of mass of outer housing

ℓ_3 = distance from lower input accelerometer to center of mass of outer housing

ℓ_4 = distance from upper input accelerometer to center of mass of outer housing

and all accelerations are in complex notation.

Assuming that the elastomer cartridges had negligible cross-coupling stiffness, K_1 and K_2 were calculated using equations (9) through (12).

$$\alpha = \left| A_{OT} / A_{IT} \right| \tag{9}$$

$$\varphi = \angle A_{OT} / A_{IT} \tag{10}$$

$$K_1 = \frac{\omega^2 M (\alpha^2 - \alpha \cos \varphi)}{\alpha^2 - 2\alpha \cos \varphi + 1} \tag{11}$$

$$K_2 = \frac{\omega^2 M \alpha \sin \varphi}{\alpha^2 - 2\alpha \cos \varphi + 1} \tag{12}$$

where α = translational transmissibility, that is the ratio of absolute values of output to input acceleration

φ = translational phase angle between input and output acceleration signals (the positive value of φ was used)

M = the value of resonant mass.

The development of equations (11) and (12) is presented in reference [3].

For reference, the minicomputer also calculated and printed out the conical motion of the inner and outer elastomer support housings using equations (13) through (16).

$$A_{IC} = (A_3 - A_4)/(\ell_3 + \ell_4) \tag{13}$$

$$A_{OC} = (A_1 - A_2)/(\ell_1 + \ell_2) \tag{14}$$

$$\alpha_c = \left|A_{OC}/A_{IC}\right| \tag{15}$$

$$\varepsilon_c = \underline{/A_{OC}/A_{OI}} \tag{16}$$

where,

A_{IC} = conical acceleration of elastomer inner housing **(rad/sec^2)**

A_{OC} = conical acceleration of elastomer outer housing **(rad/sec^2)**

α_c = conical transmissibility across elastomer cartridge

ε_c = conical phase angle across elastomer cartridge

and ℓ_1, ℓ_2, ℓ_3, ℓ_4, A_1, A_2, A_3, and A_4 are defined above.

During the course of running the tests, in cases when the minicomputer calculations indicated that the translatory response of the elastomer cartridge was not significantly higher than the conical response, the results of the stiffness and damping calculations were not considered to be accurate and were ignored.

Tests Performed

A specific plan of tests for the rotating load elastomer test rig was laid out for this test program. This plan is illustrated in Table 5. Table 5 gives a listing of the tests run. The references to amplitude in this test plan are approximate. That is, the numbers given refer to the amplitude at resonance (which dropped off to either side of resonance) and indicate a general amplitude range which was used, rather than a specific value of amplitude. This is because the amplitude was controlled by the amount of unbalance in the test rig and was affected by the elastomer properties, as well as by speed and

TABLE 5

ELASTOMER ROTATING LOAD TEST RIG TESTS

I. BUTTON CARTRIDGE #1 (0.0032 m thick)

A) 5 Microns P-P (nominal) Amplitude*

1) 7.3 Kg resonant mass (16 lbs)

2) 3.6 Kg resonant mass (8 lbs)

3) 1.8 Kg resonant mass (4 lbs)

B) 12.5 Microns P-P Amplitude - 2.2 Kg resonant mass (4.8 lbs)

C) 25 Microns P-P Amplitude - 2.2 Kg resonant mass (4.8 lbs)

II. BUTTON CARTRIDGE #2 (0.0024 m thick)

5 Microns P-P (nominal) Amplitude

1) 11.3 Kg resonant mass (25 lbs)

2) 5.0 Kg resonant mass (11 lbs)

3) 3.2 Kg resonant mass (7 lbs)

III. BUTTON CARTRIDGE #3 (0.0048 m thick)

5 Microns P-P (nominal) Amplitude

1) 2.3 Kg resonant mass (5 lbs)

2) 1.4 Kg resonant mass (3 lbs)

3) 0.9 Kg resonant mass (2 lbs)

IV. RING CARTRIDGE #1 (0.0048 m wide)

A) 5 microns P-P (nominal) Amplitude

1) 3.5 Kg resonant mass (7.8 lbs)

2) 2.2 Kg resonant mass (4.8 lbs)

3) 1.3 Kg resonant mass (2.8 lbs)

B) 12.5 Microns P-P Amplitude - 2.2 Kg resonant mass (4.8 lbs)

C) 25 Microns P-P Amplitude - 2.2 Kg resonant mass (4.8 lbs)

V. RING CARTRIDGE #2 (0.0024 m wide)

0.1 Microns P-P (nominal) Amplitude**

1) 3.5 Kg resonant mass (7.8 lbs)

2) 1.7 Kg resonant mass (3.8 lbs)

3) 0.8 Kg resonant mass (1.7 lbs)

---

*Amplitudes listed in this table are representative; since unbalance was the independent variable in each run, amplitude varied widely in the resonant region.

**See discussion of low amplitude in text.

resonant mass. The different resonant masses given in Table 5 for each cartridge were used for the purpose of getting response data at widely separated frequencies. This was necessary because the speed range over which useful data could be obtained for a single resonant condition was usually no more than about 5000 rpm.

Test Results

It is the purpose of this section to present the results of the tests performed during this investigation and compare them to the predictions of elastomer dynamic properties presented in an earlier section of this report. The method of presentation chosen is predominantly that of data plots showing measured elastomer stiffness (in N/m) and loss coefficient versus test frequency. Additional test values, specifically amplitude and phase angle, are also plotted as functions of frequency. The predicted values for stiffness and loss coefficient are also represented on the appropriate plots. Significant scatter in the measured values of stiffness and loss coefficient may be observed. Two reasons for this scatter have been hypothesized. First, the motion of the elastomer cartridge was not entirely translatory, as discussed above. Second, strain varied during the tests, as a function of frequency, due to the resonant nature of the testing. The significance of changes in strain is discussed below. To facilitate the evaluation of the test results, the results for each test are summarized in tables listing the average values of measured stiffness, damping, and loss coefficient for each resonant mass along with the appropriate predicted values.

Button Cartridge #1

This cartridge was tested initially at three different frequency ranges while keeping the peak elastomer amplitudes about the same. A second set of tests was conducted with this cartridge during which the peak amplitude was changed while the frequency range remained the same. This was accomplished by changing the unbalance weight in the test rig. The amplitude variation tests were run at the lowest of the three frequency ranges from the first set of tests. For the first set of tests for this cartridge, the frequency variation tests, the amplitude in the vicinity of resonance and phase angle of the elastomer response are plotted as a function of frequency in Figures 15 and 16, respectively. The stiffness and loss coefficient values calculated from this data

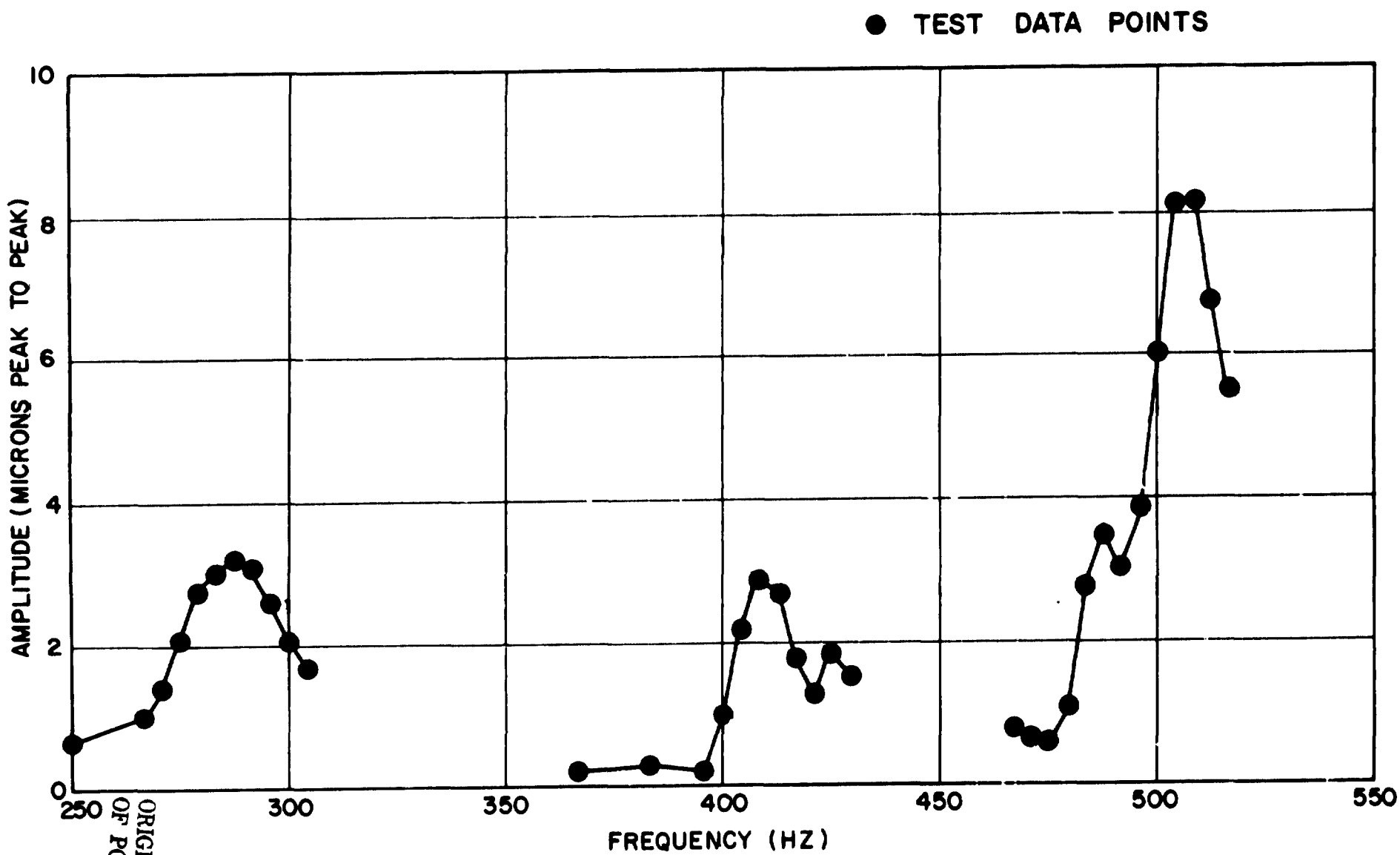

Figure 15. Amplitude Across Elastomer as a Function of Frequency for Frequency Variation Tests of Button Cartridge #1 (0.0032 m Thick)

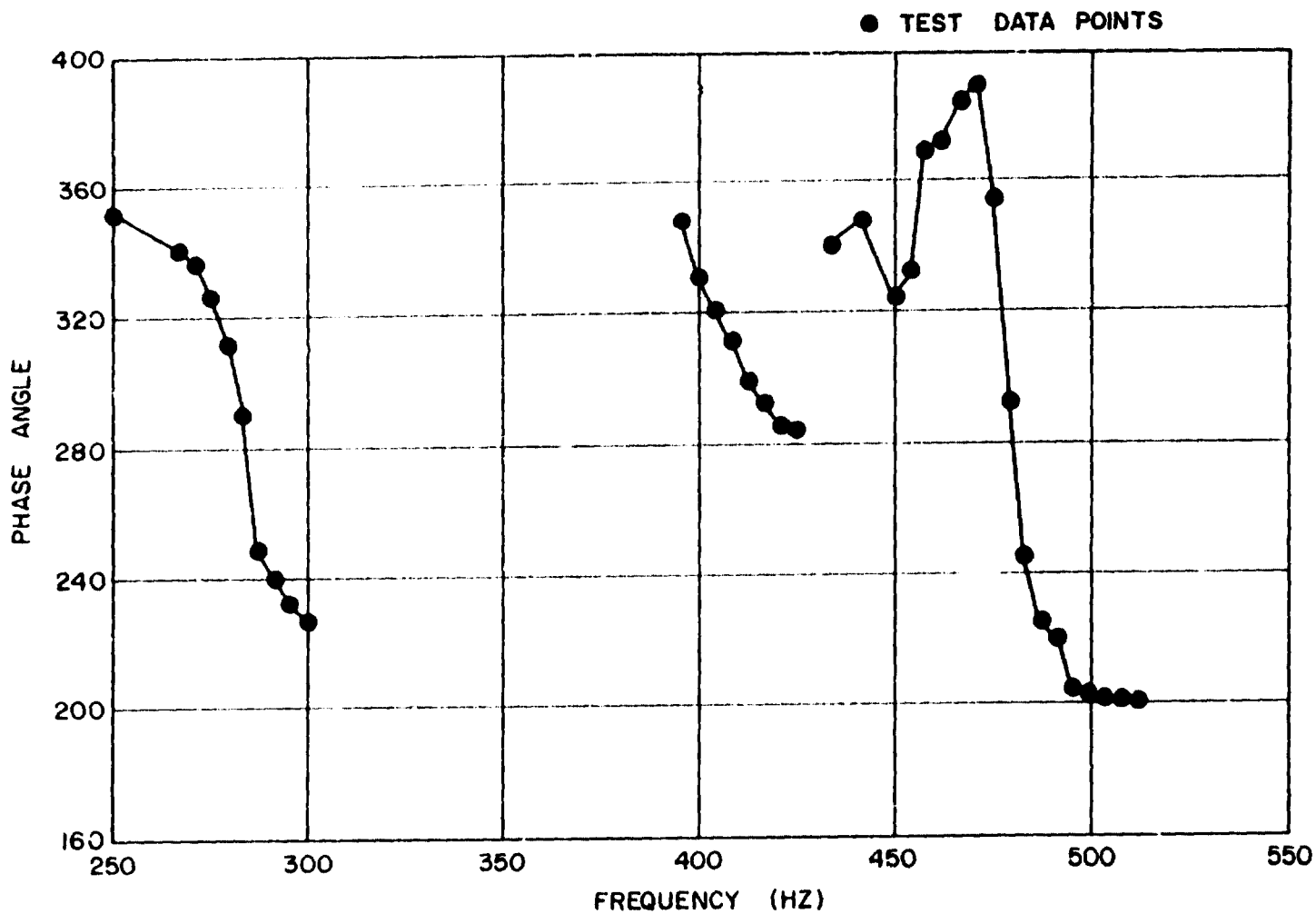

Figure 16. Phase Angle as a Function of Frequency for Frequency Variation Tests of Button Cartridge #1 (0.0032 m Thick)

are presented on log-log plots as functions of frequency, in Figure 17. The predicted values of stiffness and loss coefficient, both including and neglecting the effect of shear loading of the buttons, are shown in Figure 17 for comparison with the test results. Since the buttons in this cartridge were glued in place on both sides, it was expected that they would undergo shear as well as compression loading. Table 6 presents the average measured values of stiffness, damping, and loss coefficient for each of the frequency variation tests and the predicted values for each, both including and neglecting shear. The measured stiffness agrees quite favorably with the predictions that include the effect of shear. At the lower frequencies, the measured stiffness was slightly higher than the predicted value including the effect of shear, while at the highest frequencies, the measured value was slightly lower than the predicted value. For example, at 280 Hz, the measured stiffness is 2.123×10^7 N/m and the predicted value is 1.655×10^7 N/m, while at 480 Hz, the measured stiffness is 1.586×10^7 N/m and the predicted value is 1.720×10^7 N/m. However, the measured damping (and subsequently the measured loss coefficient) agrees with the predictions only for the low frequency test results. At 280 Hz, the measured value for damping was 5.386×10^6 N/m and is close to the predicted value of 4.023×10^6 N/m, while the measured value for loss coefficient was 0.2538, which is very close to the predicted value of 0.2416. At higher frequencies, there is significant scatter; the 410 Hz damping results are regarded as anomalous. At 480 Hz, the measured damping value of 1.277×10^6 N/m is much less than the predicted value of 3.794×10^6 N/m, while the measured loss coefficient of 0.0851 is also much less than the predicted value of 0.2206. However, extrapolating the curves from Figure 12 (reproduced from reference 3), the value of loss coefficient predicted on the basis of strain is about 0.1 for a compression specimen and about 0.14 for a cartridge specimen. These values compare more favorably with the 480 Hz results than with the 280 Hz results.

The results for the amplitude variation tests for Button Cartridge #1 are presented in a similar form in Figures 18 through 20 and in Table 7. Since the prediction equations for stiffness and damping do not consider the effect of strain, the corresponding predictions in Table 7 do not reflect any dependence on strain. The measured values of stiffness fell slightly at higher strains, a trend consistent with results of reference [3]. At a strain of 0.002 the measured stiffness was 2.123×10^7 N/m. The measured stiffness was

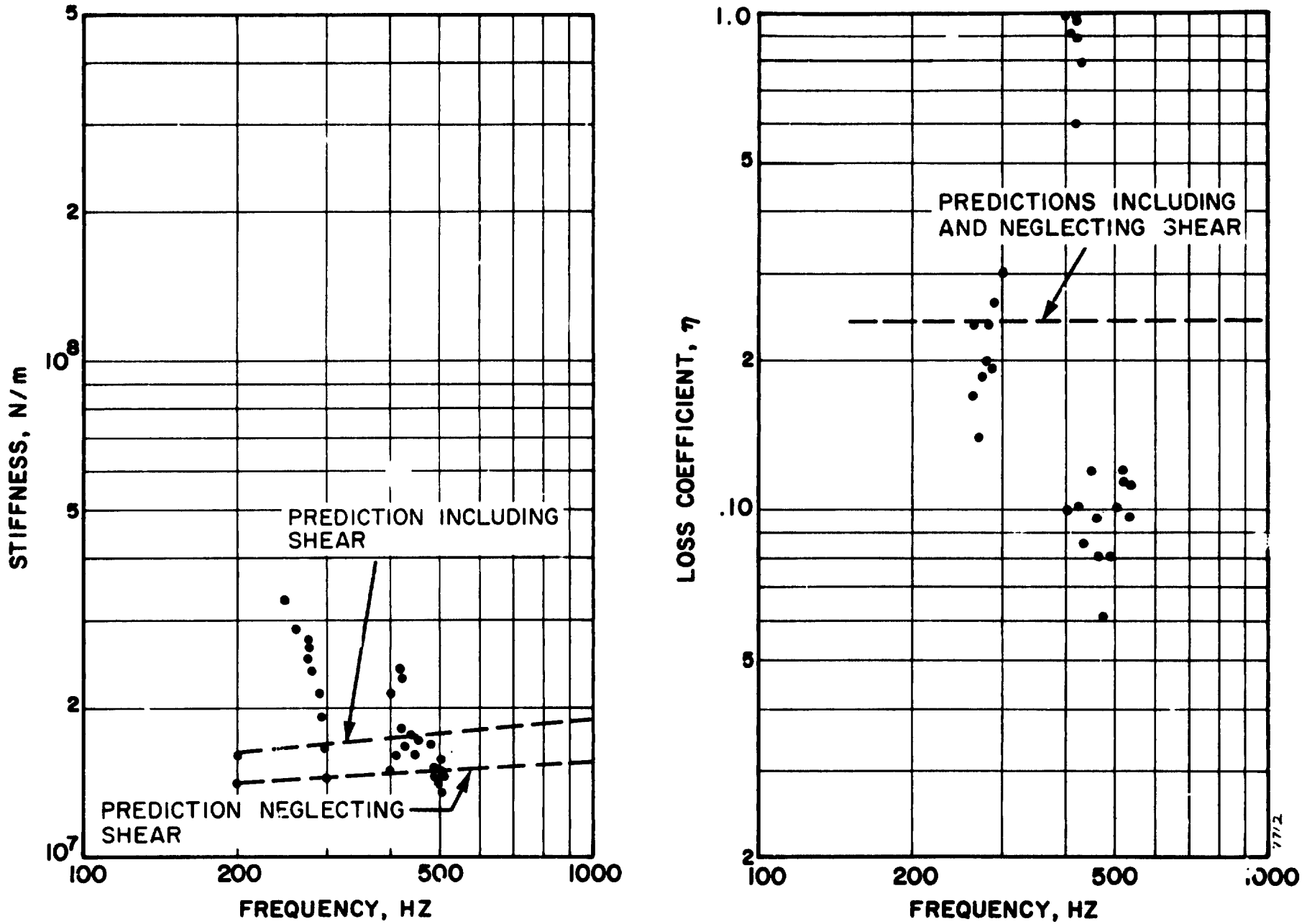

Figure 17. Stiffness and Loss Coefficient of Button Cartridge #1 (0.0032 m Thick) for Frequency Variation Tests as a Function of Frequency

TABLE 6

ELASTOMER ROTATING RIG TEST RESULTS AND PREDICTIONS FOR FREQUENCY VARIATION TESTS OF BUTTON CARTRIDGE #1 (0.0032 m THICK)

Frequency (HZ) Average*	Stiffness (MN/m)			Damping (MN/m)			Loss Coefficient		
	Average* Measured	Predicted With Shear	Predicted Without Shear	Average* Measured	Predicted With Shear	Predicted Without Shear	Average* Measured	Predicted With Shear	Predicted Without Shear
280	21.2	16.7	14.6	5.390	4.02	3.64	0.254	0.242	0.252
410	20.7	17.0	14.8	21.380	3.86	3.49	1.030	0.227	0.235
480	15.9	17.2	14.9	1.277	3.79	3.44	0.085	0.221	0.230

*For each resonant mass

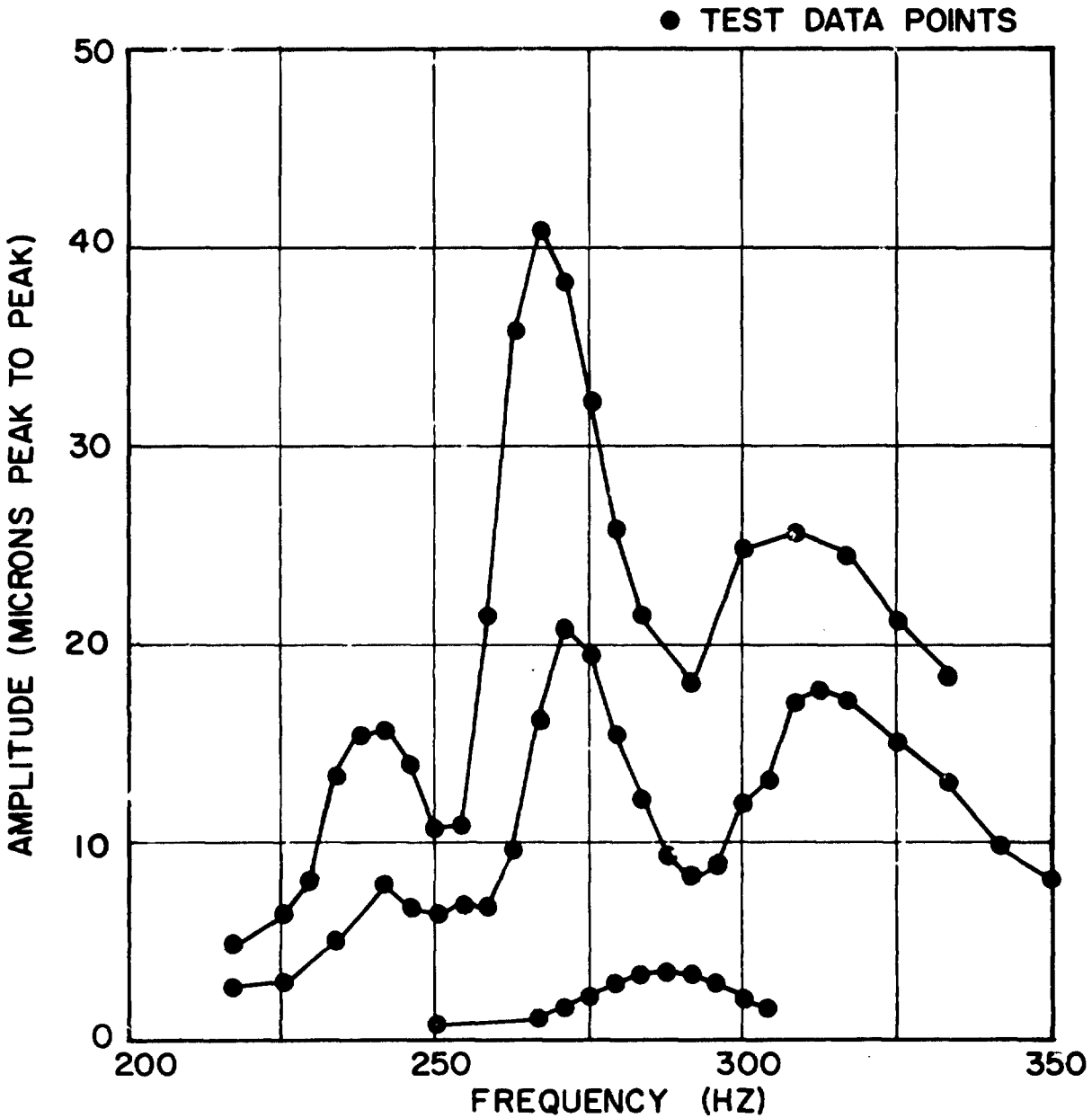

Figure 18. Amplitude Across Elastomer as a Function of Frequency for Amplitude Variation Tests of Button Cartridge #1 (0.0032 m Thick)

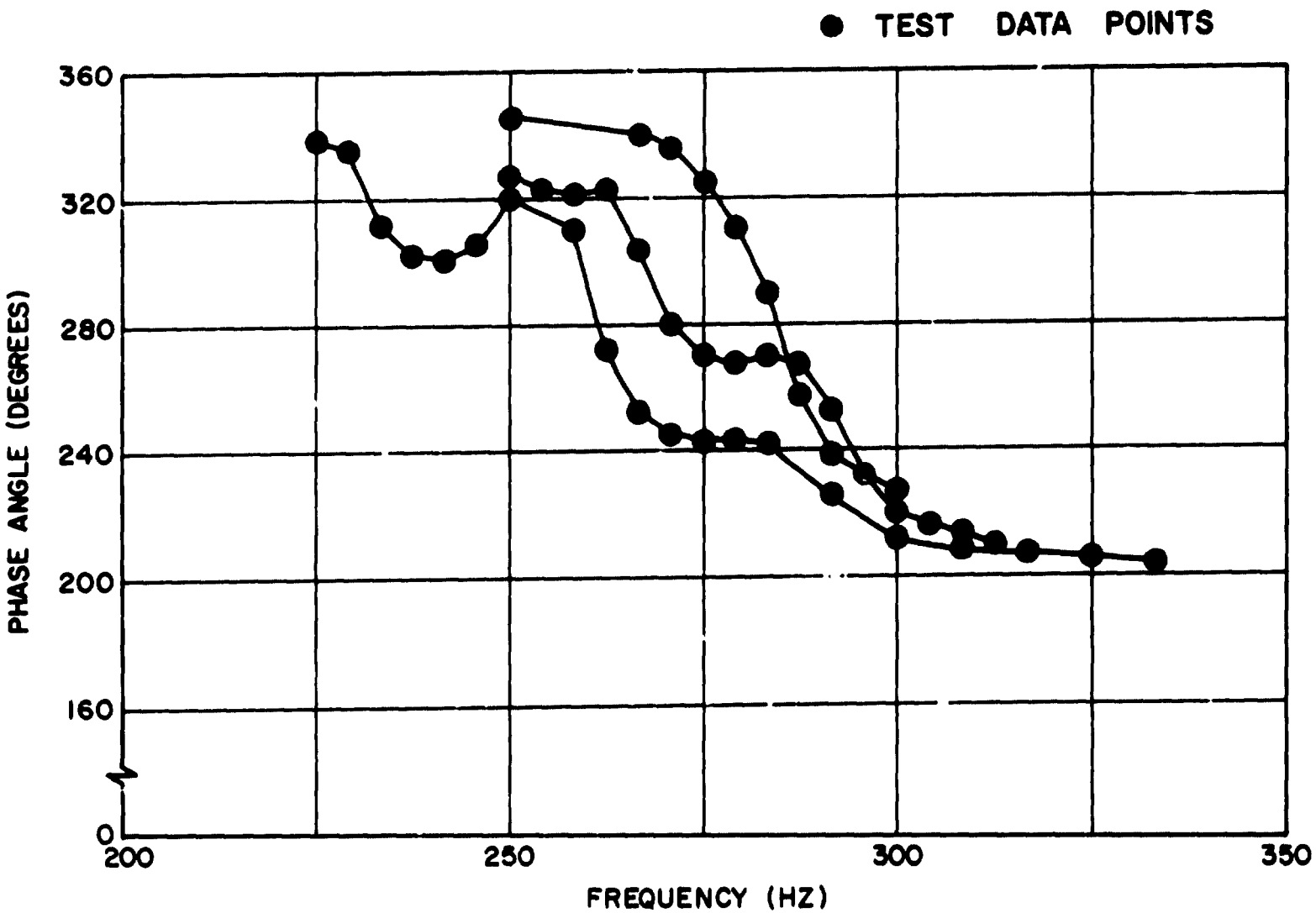

Figure 19. Phase Angle as a Function of Frequency for Amplitude Variation Tests of Button Cartridge #1 (0.0032 m Thick)

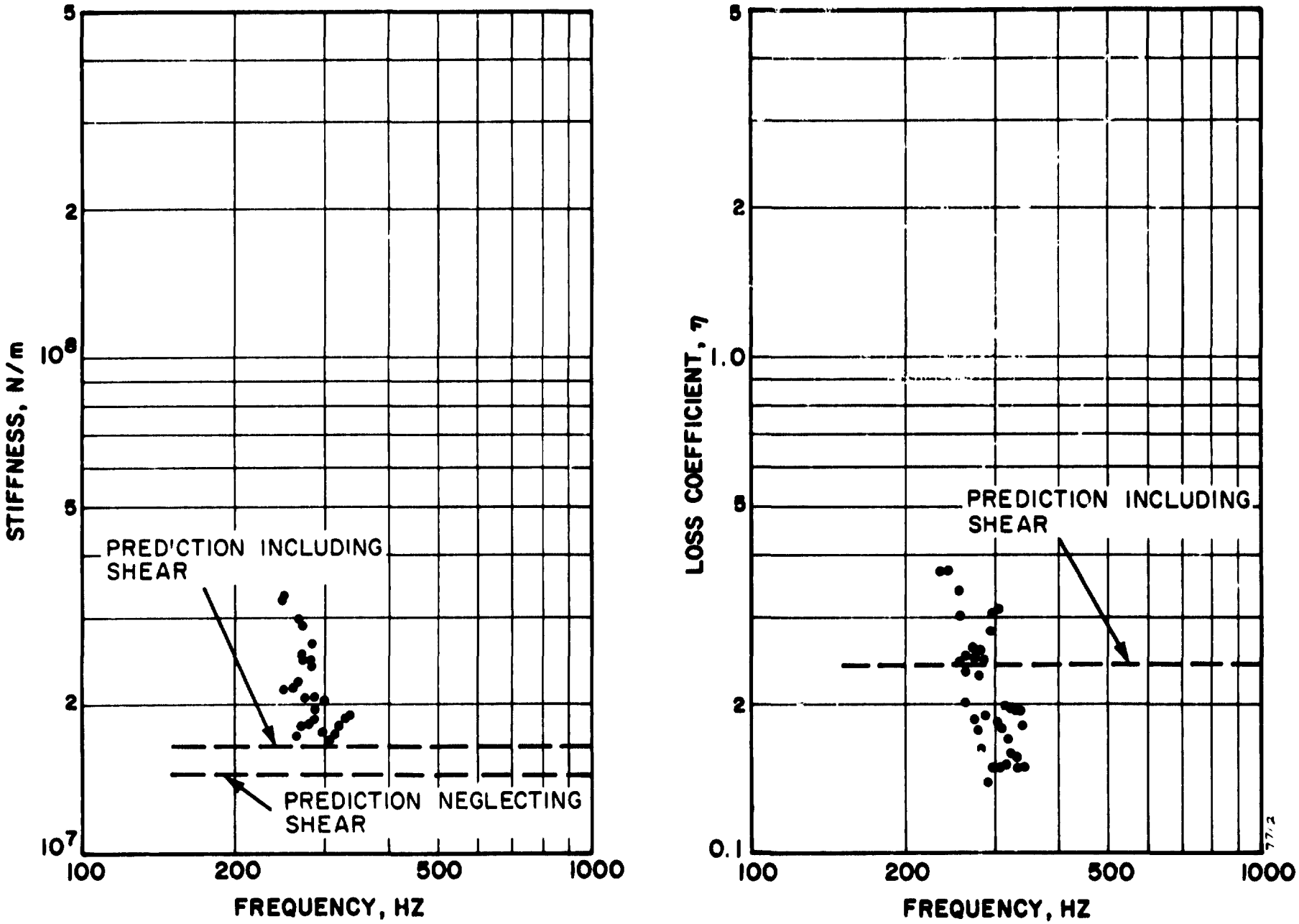

Figure 20. Stiffness and Loss Coefficient of Button Cartridge #1 (0.0032 m Thick) for Amplitude Variation Tests as a Function of Frequency

TABLE 7

ELASTOMER ROTATING RIG TEST RESULTS AND PREDICTIONS FOR AMPLITUDE VARIATION TESTS OF BUTTON CARTRIDGE #1 (0.0032 m THICK)

Peak Double Amplitude Strain (m/m)	Stiffness (MN/m)			Damping (MN/m)			Loss Coefficient		
	Average* Measured	Predicted With Shear	Predicted Without Shear	Average* Measured	Predicted With Shear	Predicted Without Shear	Average* Measured	Predicted Variable Strain	Predicted With Shear
0.002	21.2	16.7	14.6	5.39	4.02	3.64	0.254	0.10	0.242
0.006	21.5	16.7	14.6	4.17	4.02	3.64	0.194	0.19	0.242
0.013	18.2	16.7	14.6	4.31	4.02	3.64	0.236	0.21	0.242

*For each change in rotating unbalance

virtually unchanged at a strain of 0.006 with a value of 2.147×10^7 N/m. At a strain of 0.016, the measured stiffness dropped to 1.821×10^7 N/m, which was approaching the strain-independent predicted value 1.665×10^7 N/m. Contrary to other results to be discussed, the measured values of damping were consistently higher than the predicted values. For the three values of strain the measured damping values were 5.386×10^6 N/m, 4.174×10^6 N/m, and 4.305×10^6 N/m as compared to the predicted value of 4.023×10^6 N/m. The loss coefficient was predicted in two different ways: first, from Figure 12 (which is reproduced from reference 3) as a function of strain, independent of geometry and frequency; and second, as a ratio of the predicted values of stiffness and damping, including the effect of shear, as done for the frequency variation tests. This second method does not consider the effect of strain, which has been shown to be significant. Except for the lowest strain case, with a measured loss coefficient of 0.2538 compared to a prediction from Figure 12 of about 0.1, the measured values are close to the loss coefficient predictions from Figure 12. For a strain of 0.006, the measured loss coefficient of 0.19 is virtually identical to the predicted value. Meanwhile, for a strain of 0.013, the measured value of 0.2364 was close to the prediction from Figure 12 of about 0.21 and approached the strain independent prediction of 0.2416.

Button Cartridge #2

Only frequency variation tests were conducted with the cartridge. The results for these tests are presented in Figures 21 through 23 and in Table 8. The predictions for elastomer stiffness were generally higher than the measured values. For example, at 425 Hz, compare the measured stiffness value of 3.59×10^7 N/m with the predicted value, including the effect of shear, of 3.132×10^7 N/m. The measured values of damping (and subsequently the loss coefficient) were only about half of the predicted values. To be specific, also at 425 Hz, the measured values of damping and loss coefficient were 3.928×10^6 N/m and 0.1094, as compared to predicted values of 7.601×10^6 N/m and 0.2427, respectively. Although these measured damping and loss coefficient values were lower than the predicted values, they were quite consistent. Therefore, it is reasonable to assume that they are the result of the low strain levels involved in the testing. In fact, the loss coefficient prediction based on extrapolation

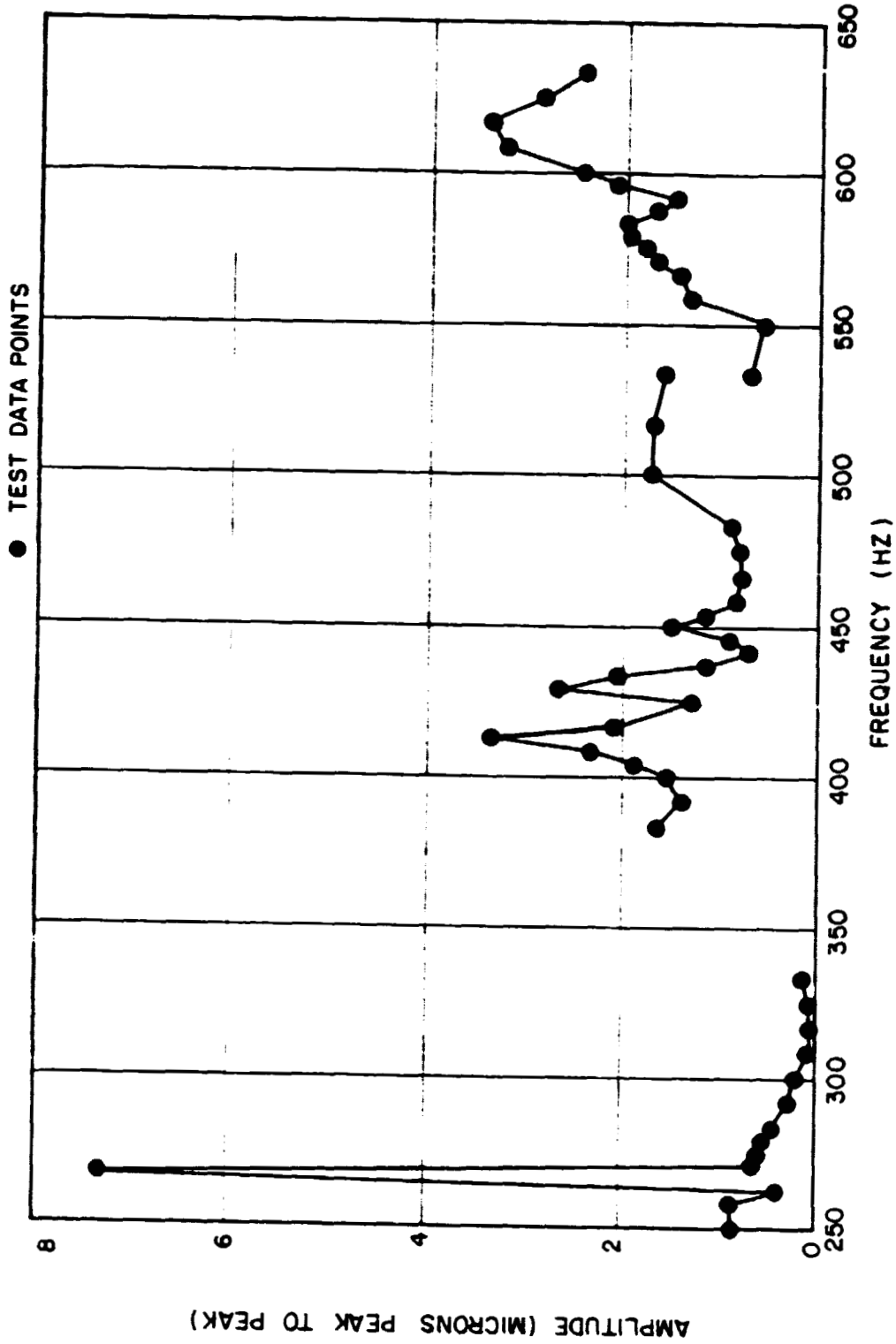

Figure 21. Amplitude Across Elastomer as a Function of Frequency for Button Cartridge #2 (0.0024 in Thick)

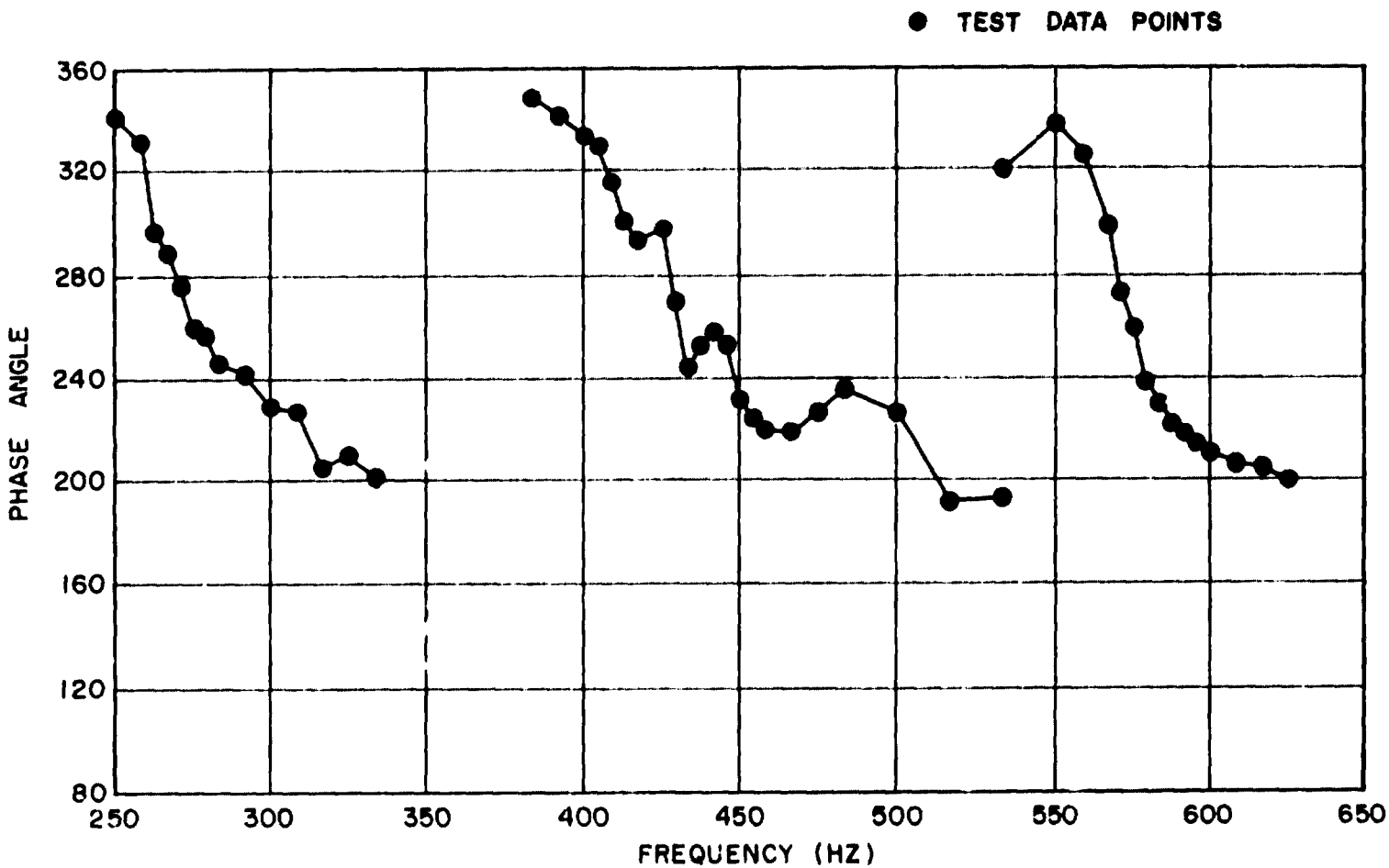

Figure 22. Phase Angle as a Function of Frequency for Button Cartridge #2 (0.0024 m Thick)

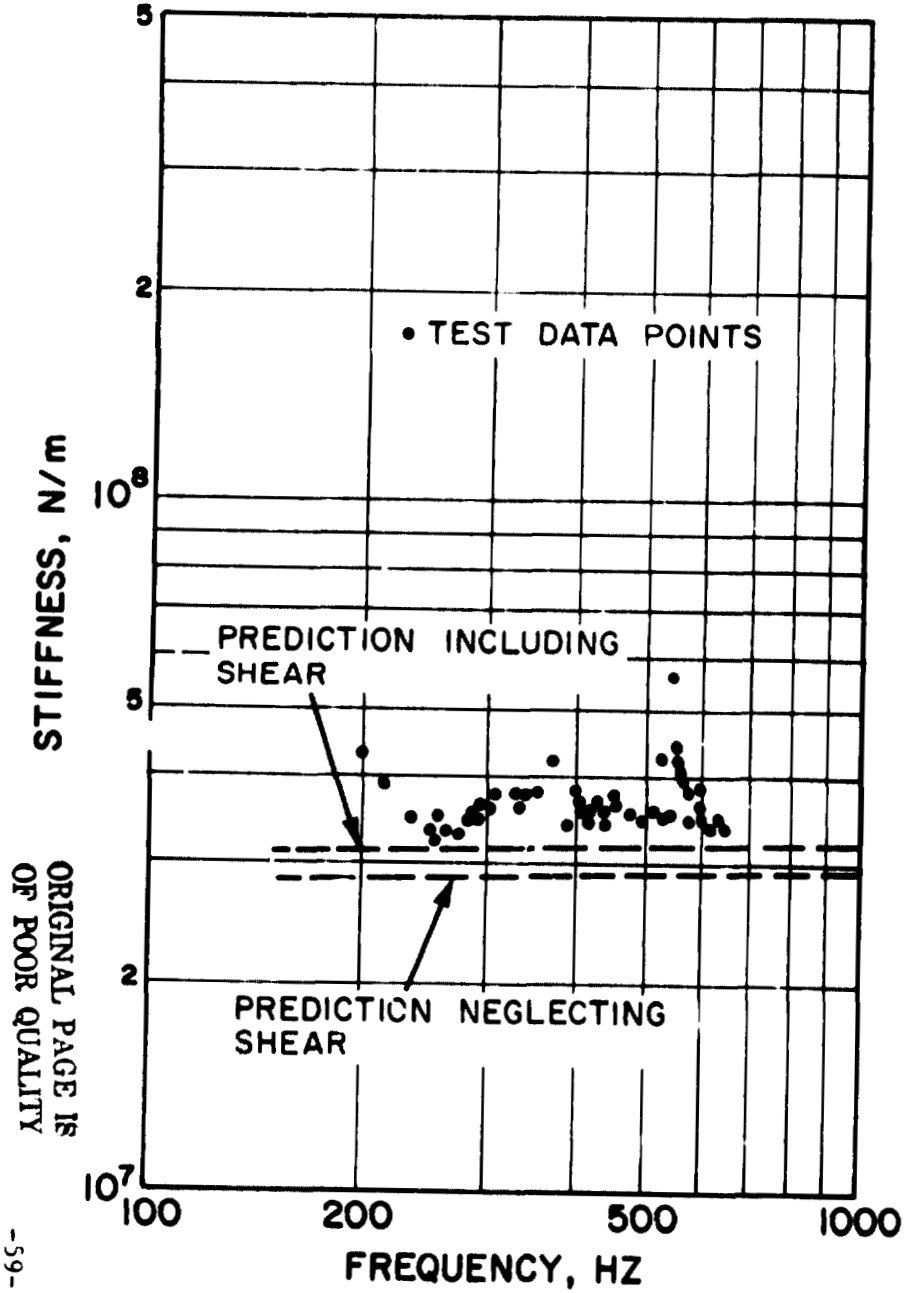

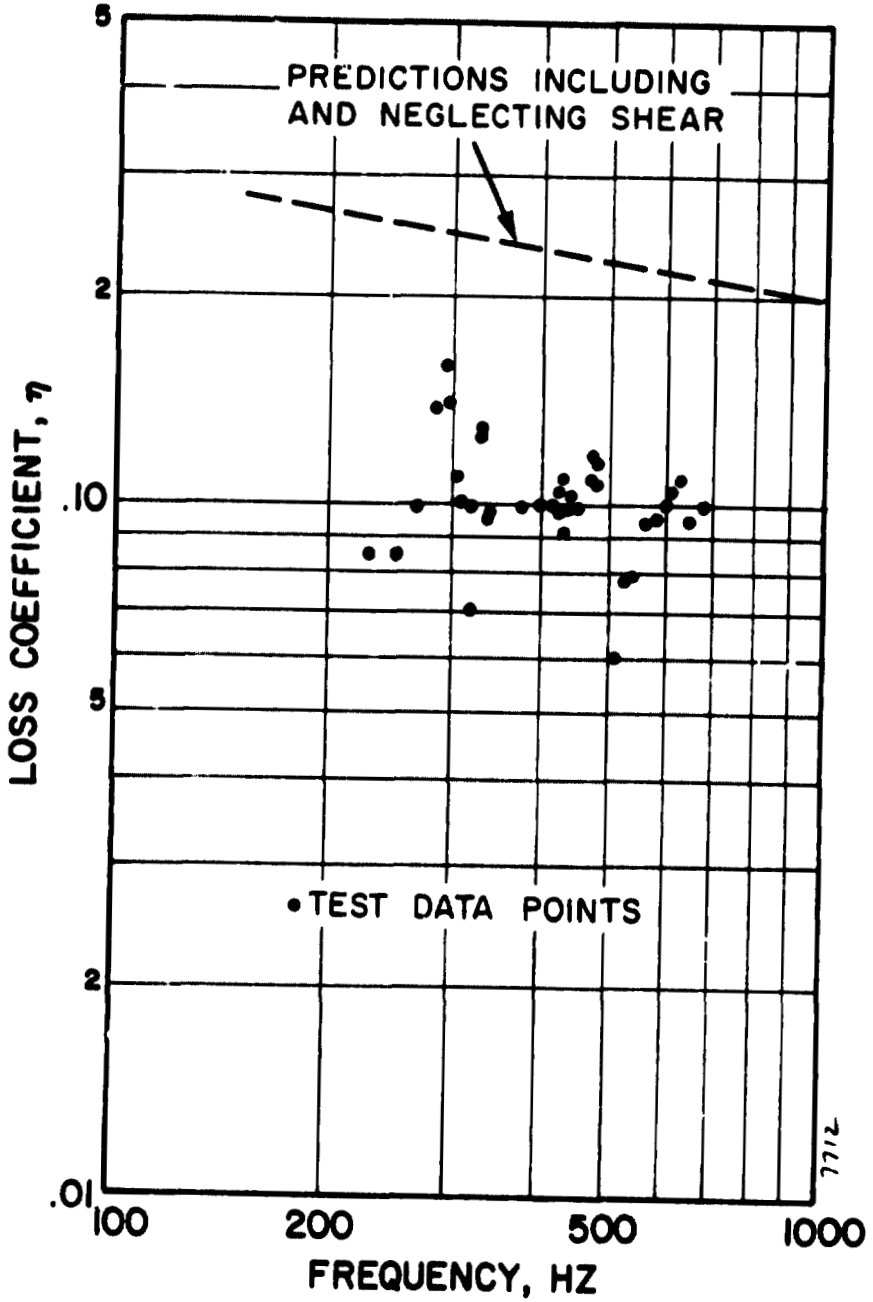

Figure 23. Stiffness and Loss Coefficient of Button Cartridge #2 (0.0024 m Thick) as a Function of Frequency

TABLE 8
ELASTOMER ROTATING RIG TEST RESULTS AND PREDICTIONS
FOR BUTTON CARTRIDGE #2 (0.0024 m THICK)

Frequency (Hz) Average*	Stiffness (MN/m)			Damping (MN/m)			Loss Coefficient		
	Average* Measured	Predicted Without Shear	Predicted With Shear	Average* Measured	Predicted Without Shear	Predicted With Shear	Average* Measured	Predicted Without Shear	Predicted With Shear
275	35.6	28.4	3.11	3.71	7.45	7.96	0.104	0.262	0.256
425	35.9	28.4	3.13	3.93	7.12	7.60	0.109	0.251	0.243
575	39.4	28.4	3.16	4.30	6.90	7.36	0.109	0.242	0.233

*For each resonant mass

of the curves in Figure 12 is about 0.10. This is precisely the value of loss coefficient which was measured for Button Cartridge #2.

Button Cartridge #3

The amplitude in the vicinity of resonance and phase angle of the elastomer response for this cartridge are plotted as a function of frequency in Figures 24 and 25, respectively. The stiffness and loss coefficient values determined from this data are presented on log-log plots, as functions of frequency, in Figure 26. The predicted values of stiffness and loss coefficient, both including and neglecting shear effects, are shown in Figure 26 for comparison with the test results. Table 9 presents the average measured values of stiffness, damping, and loss coefficient for each of the resonant mass tests, and the predicted values for each, both including and neglecting shear effects. The test results for stiffness, as compared with the predicted values neglecting shear effects, are encouraging. Since the buttons were not, in this case, glued to the outer housing, it is reasonable that the effect of shear is not large. At 350 Hz the measured value of 6.53×10^6 N/m compares very favorably with the predicted value of 6.716×10^6 N/m. The predicted values for damping and loss coefficient are somewhat high. For example, at 350 Hz, the measured value of damping of 8.15×10^5 N/m is considerably lower than the predicted value of 1.468×10^6 N/m and the measured value of loss coefficient of 0.125 is lower than the predicted value of 0.219. However, these discrepancies can be explained by the fact that the predictions are based on moderate values of strain (e.g., 0.01) while the value of strain for these tests was very low (about 0.001). For polybutadiene, both damping and loss coefficients are known to fall with low values of strain. In fact, referring to Figure 12 for a strain of 0.001, the loss coefficient for buttons would be expected to be around 0.1 (extrapolating the curves). This value compares much more favorably with the measured value of loss coefficient in the present test series (0.125).

Ring Cartridge #1

Both frequency variation and amplitude variation tests were conducted with this cartridge. The results for the frequency variation tests are presented in Figures 27 through 29 and in Table 10. The measured data fall generally between the Gobel and Beam/Column predictions and are quite consistent. For

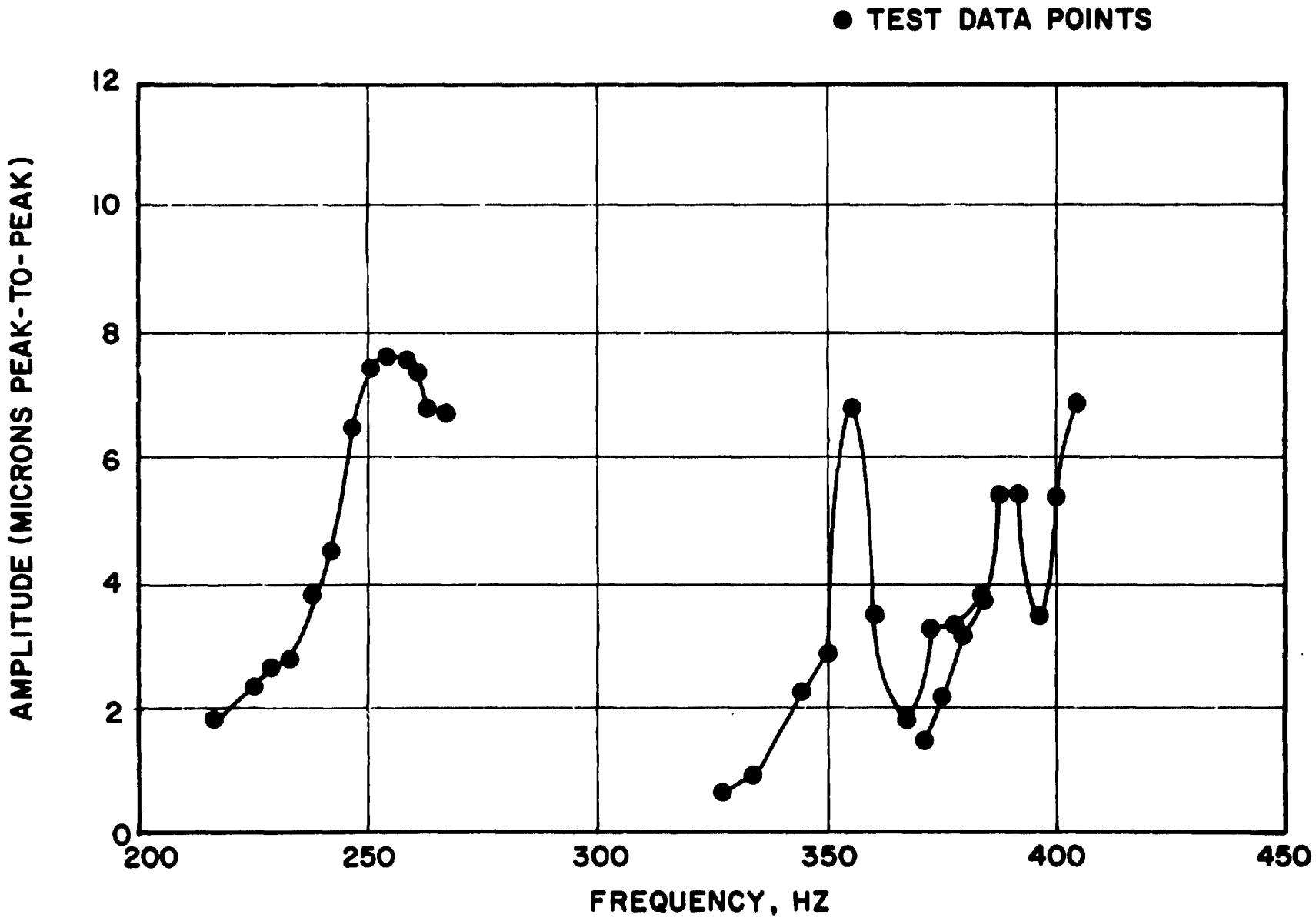

Fig. 24 Amplitude Across Elastomer as a Function of Frequency for Button #3 (0.0048 m High)

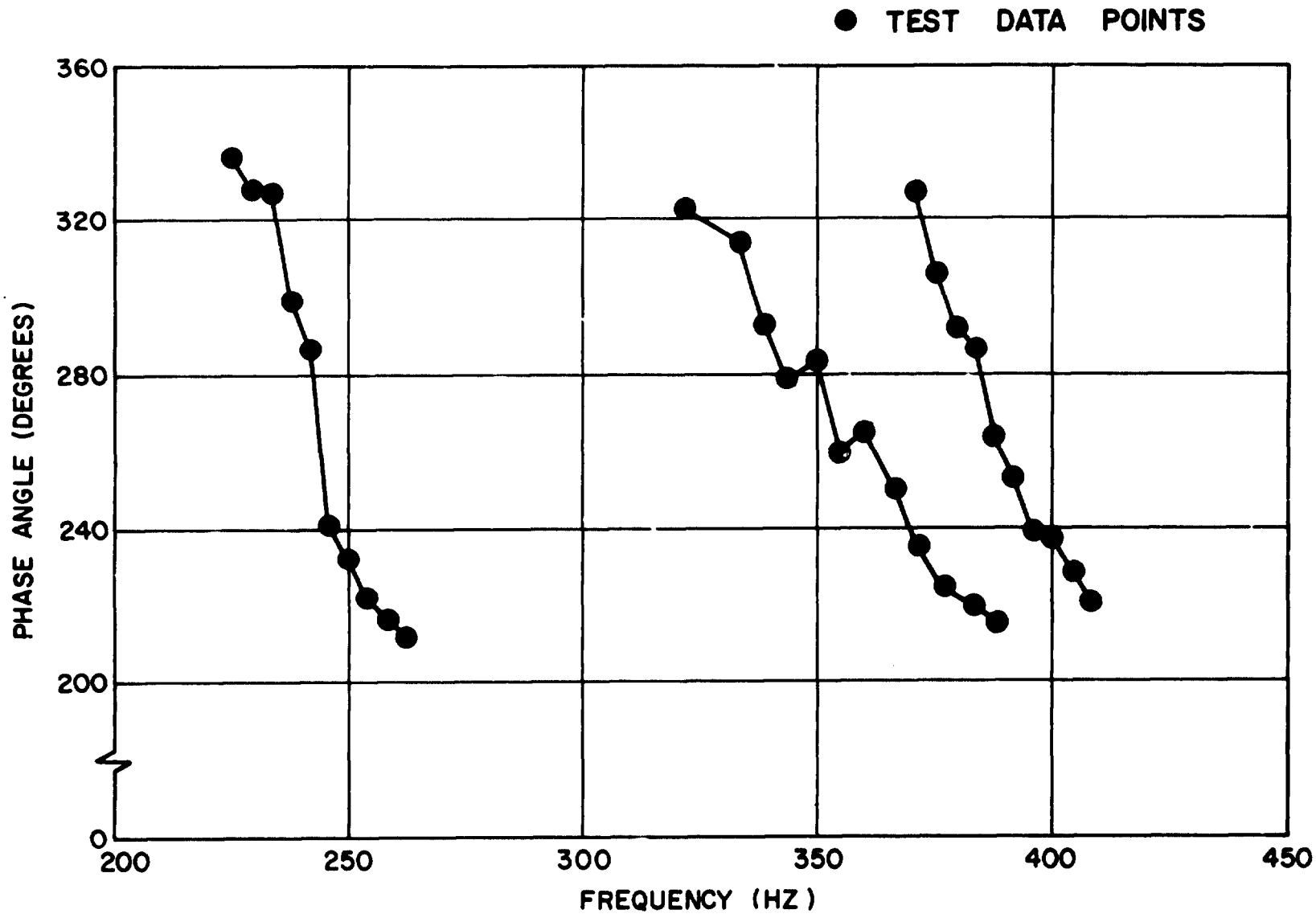

Figure 25. Phase Angle as a Function of Frequency for Button #3 (0.0048 m High)

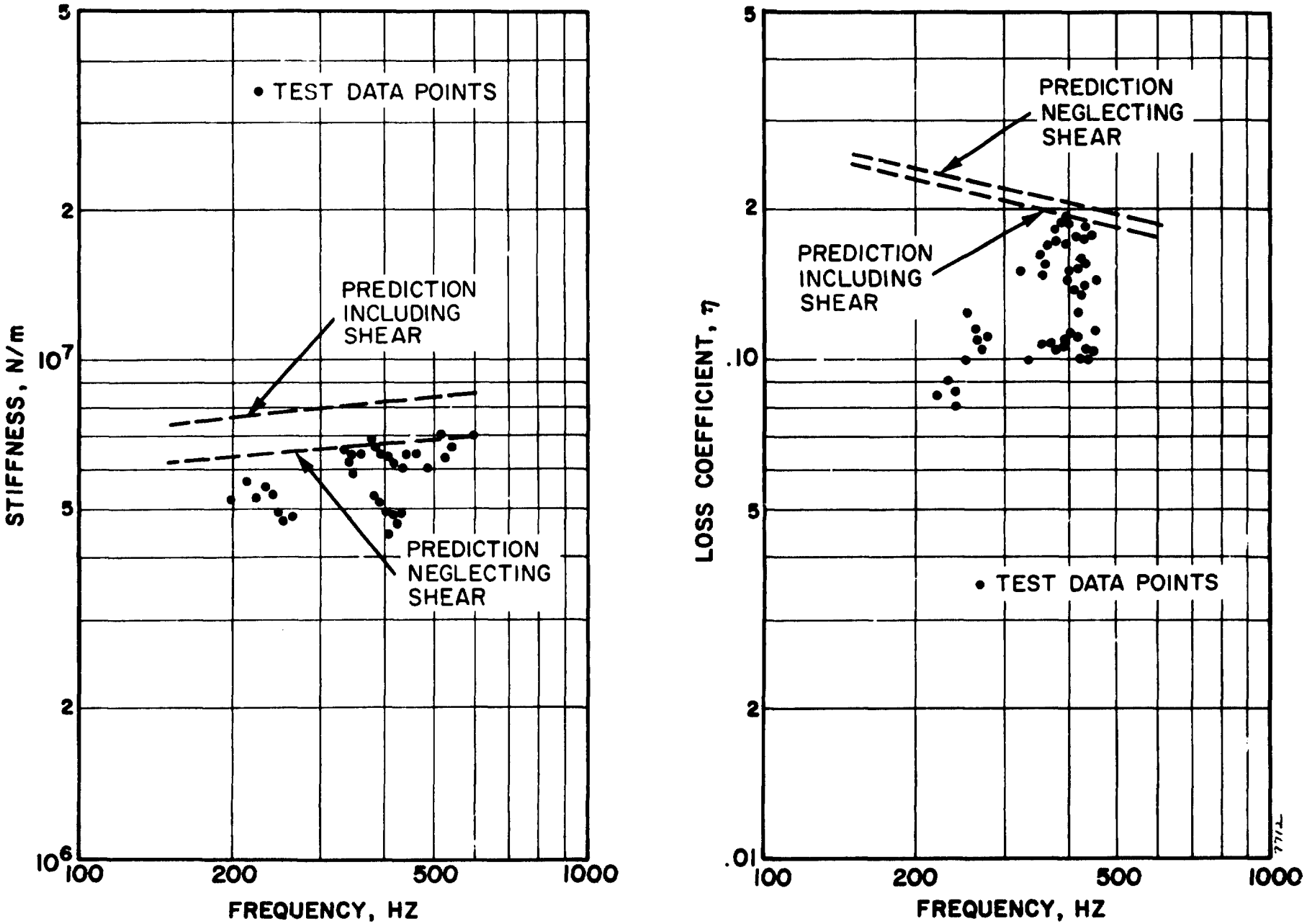

Figure 26. Stiffness and Loss Coefficient of Button Cartridge #3 (0.0048 m Thick) as a Function of Frequency

TABLE 9

ELASTOMER ROTATING RIG TEST RESULTS AND PREDICTIONS FOR BUTTON CARTRIDGE #3 (0.0048 m THICK)

Frequency (Hz) Average*	Stiffness (MN/m)			Damping (MN/m)			Loss Coefficient		
	Average* Measured	Predicted With Shear	Predicted Without Shear	Average* Measured	Predicted With Shear	Predicted Without Shear	Average* Measured	Predicted With Shear	Predicted Without Shear
250	5.12	7.82	6.51	0.551	1.78	1.52	0.108	0.228	0.234
350	6.53	8.12	6.72	0.815	1.72	1.47	0.125	0.211	0.219
420	5.02	8.30	6.84	0.835	1.68	1.44	0.166	0.202	0.210

*For each resonant mass

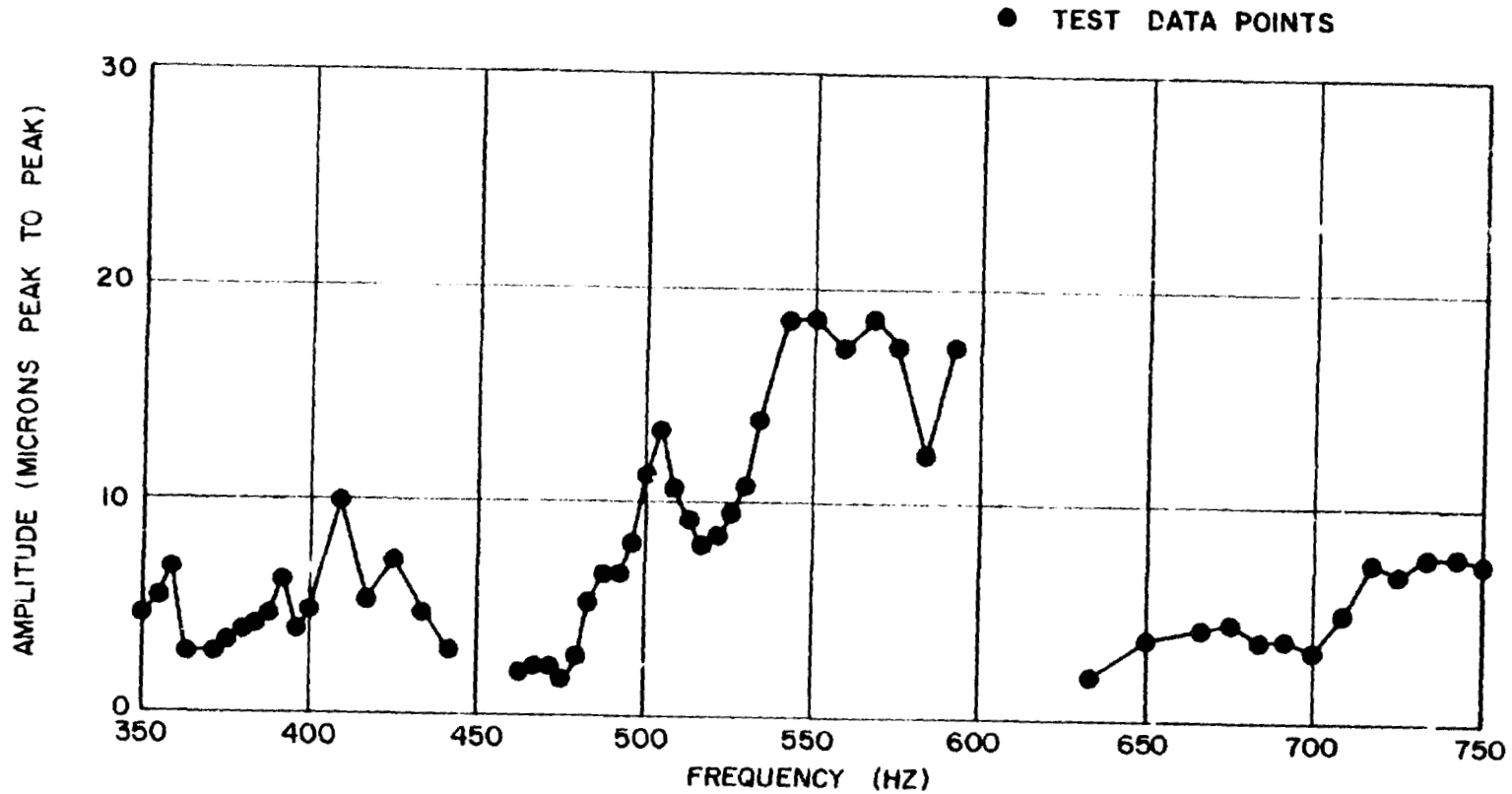

Figure 27. Amplitude Across Elastomer as a Function of Frequency for Frequency Variation Tests of Ring Cartridge #1 (0.0048 m Wide)

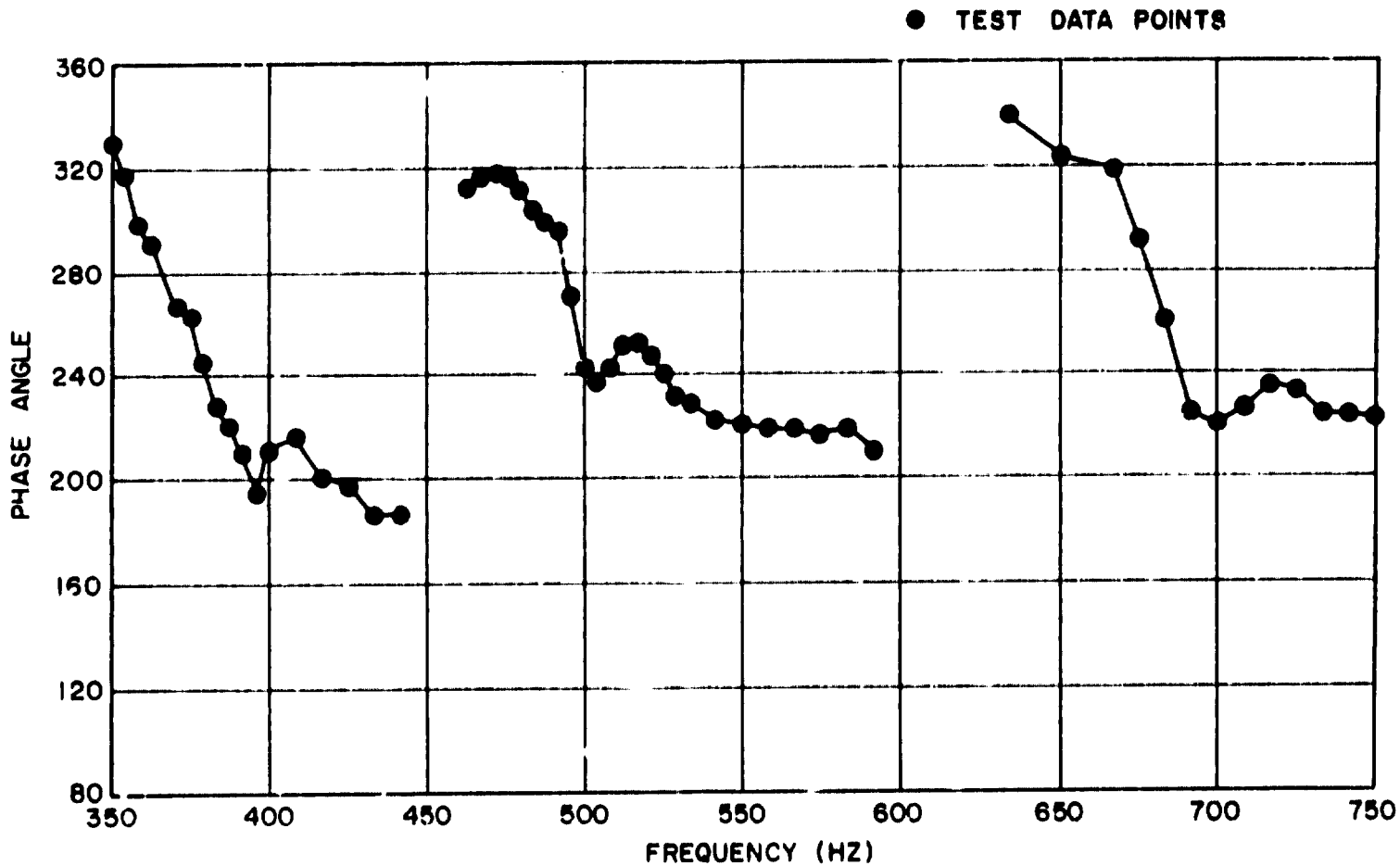

Figure 28. Phase Angle as a Function of Frequency for Frequency Variation Tests of Ring Cartridge #1 (0.0048 m Wide)

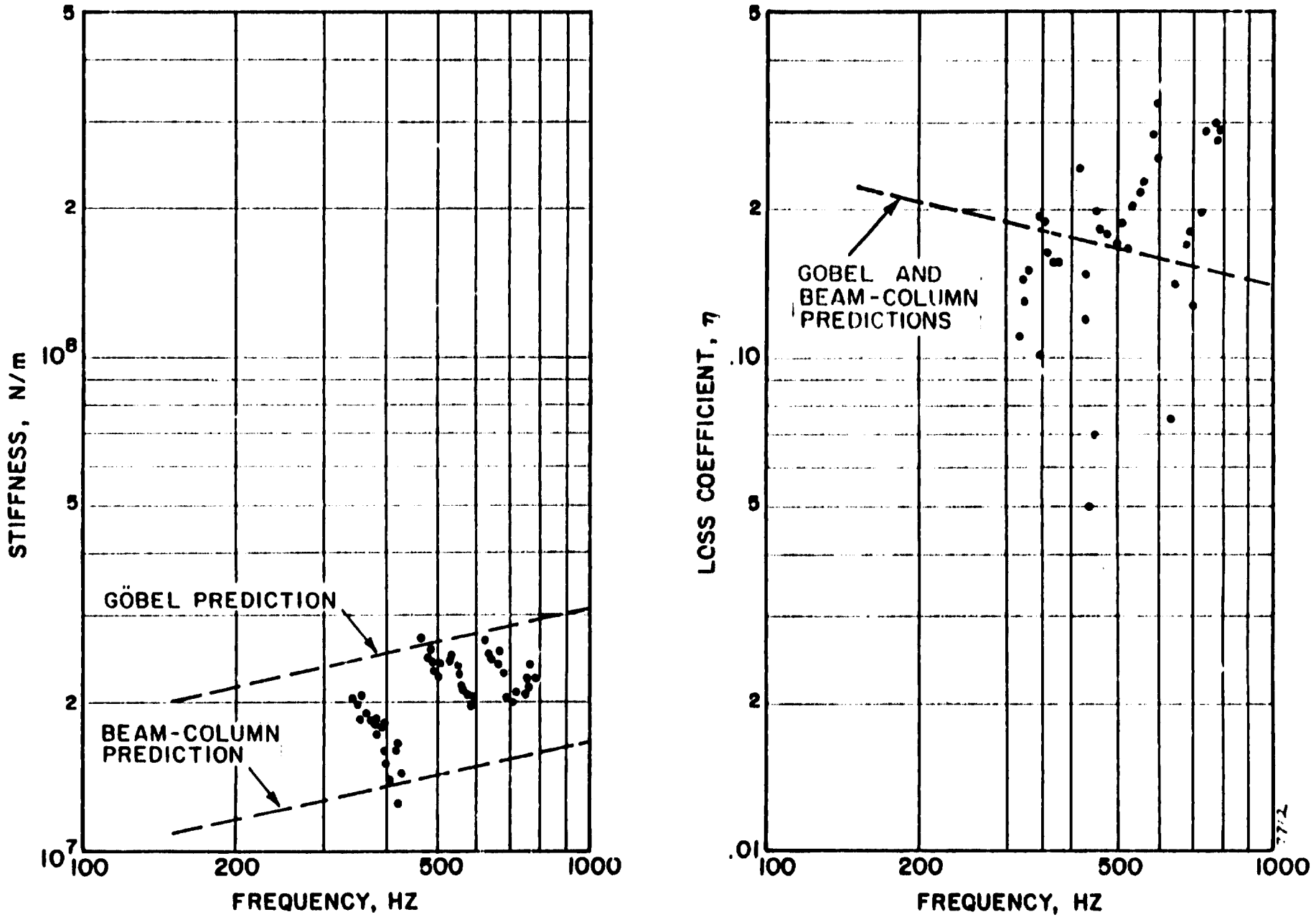

Figure 29. Stiffness and Loss Coefficient of Ring Cartridge #1 (0.0048 m Wide) for Frequency Variation Tests as a Function of Frequency

TABLE 10

ELASTOMER ROTATING RIG TEST RESULTS AND PREDICTIONS FOR FREQUENCY VARIATION TESTS OF RING CARTRIDGE #1 (0.0048 m THICK)

Frequency (Hz) Average*	Stiffness (MN/m)			Damping (MN/m)			Loss Coefficient		
	Average* Measured	Predicted Beam Column	Predicted Göbel	Average* Measured	Predicted Beam Column	Predicted Göbel	Average* Measured	Predicted Beam Column	Predicted Göbel
375	17.8	13.2	25.0	2.19	2.37	4.48	0.123	0.179	0.179
500	19.8	14.0	26.5	3.50	2.29	4.33	0.177	0.163	0.163
680	22.1	14.9	28.2	3.81	2.21	4.17	0.173	0.148	0.148

*For each resonant mass

example, at 500 Hz, the measured stiffness value of 1.977×10^7 N/m is almost exactly midway between the Beam-Column and Göbel predictions of 1.403×10^7 N/m and 2.650×10^7 N/m, respectively. The measured damping value of 3.503×10^6 N/m, at the same frequency, is also nearly midway between the Beam-Column and Göbel predictions of 2.290×10^6 N/m and 4.326×10^6 N/m, respectively. The measured loss coefficient of 0.1772 is similar to the strain-independent predicted value of 0.1632. The strain in this case was 0.004 - perhaps high enough to correspond to the value from which the strain independent prediction was developed (~.01). The results for the amplitude variation tests conducted at 500 Hz are presented in Figures 30 through 32 and in Table 11. The average measured results for stiffness and damping consistently fall between the Göbel and Beam-Column predictions. In addition, measured stiffness decreases slightly with increasing strain, as was expected, with values of 2.357×10^7 N/m, 1.977×10^7 N/m, and 1.758×10^7 N/m for strains of 0.001, 0.004, and 0.006, respectively. The measured damping values increased slightly as strain increased, up to a point, beyond which the damping began to decrease. Specifically, the measured damping values were 3.193×10^6 N/m, 3.503×10^6 N/m, and 3.389×10^6 N/m for the increasing values of strain listed above. In this case, the measured values of loss coefficient followed the expected trend and increased with increasing values of strain and also compared quite favorably with the loss coefficient predictions based on Figure 12. In particular, for a strain of 0.001, the measured loss coefficient of 0.135 was essentially identical to the prediction of 0.14, while for higher strains the measured values of loss coefficient are 15 percent below the predicted values.

Ring Cartridge #2

For Ring Cartridge #2 the amplitude in the vicinity of resonance and phase angle of the elastomer response are plotted as a function of speed in Figures 33 and 34, respectively. About each resonance, the elastomer amplitude plots (figure 33) exhibit three distinct peaks. In general, the first peak was at somewhat less than ninety degrees phase angle, and the third peak at more than one hundred degrees phase angle. These multiple peaks were apparently due to interactions between more than one mode of vibration in the elastomer specimen, as well as in the test rig itself. The source of this effect was probably interaction of translatory and conical motion of the upper bearing housing or of the elastomer cartridge itself. Also, the phase angle plot for the lowest

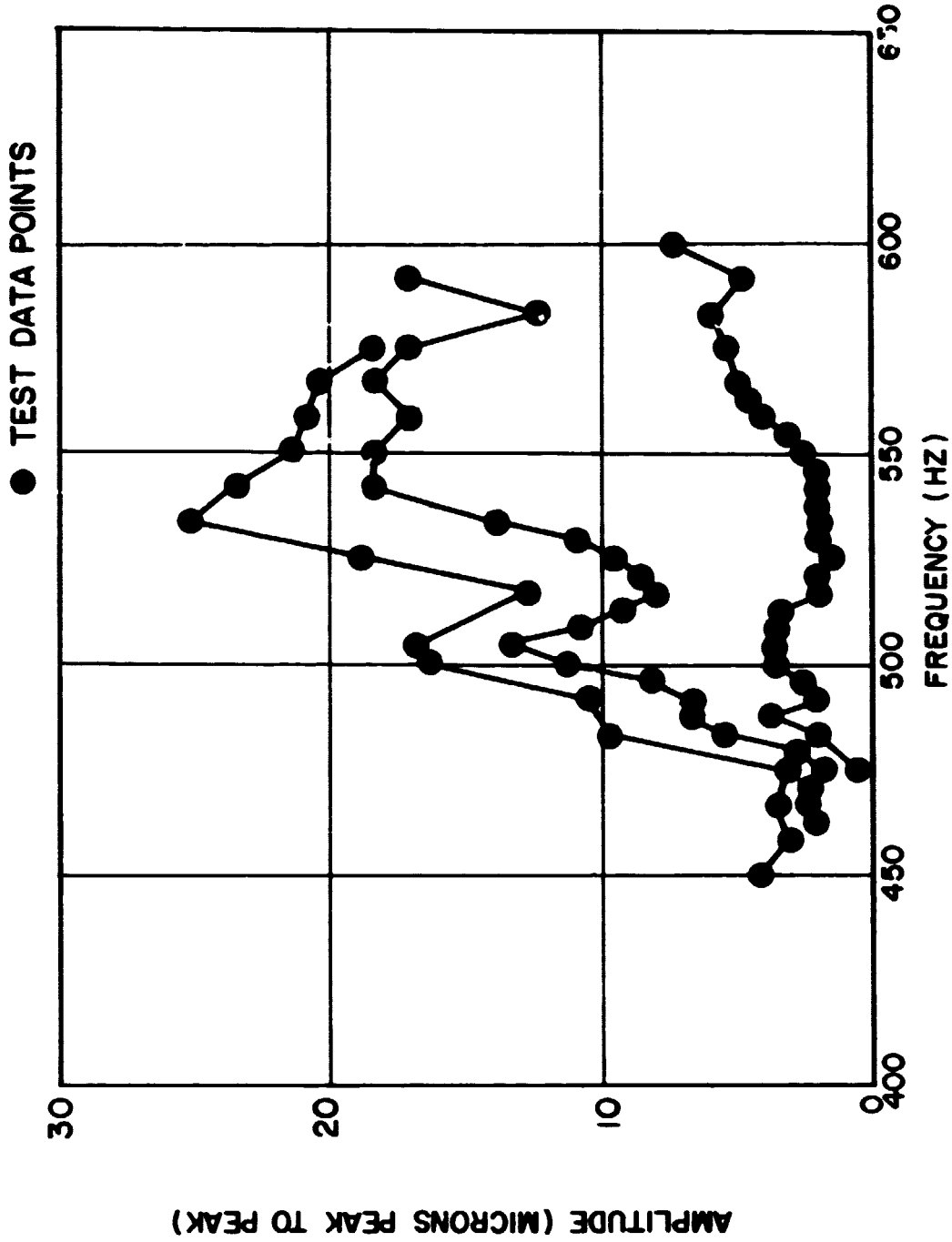

Figure 30. Amplitude Across Elastomer as a Function of Frequency for Amplitude Variation Tests of Ring Cartridge #1 (0.0048 m Wide)

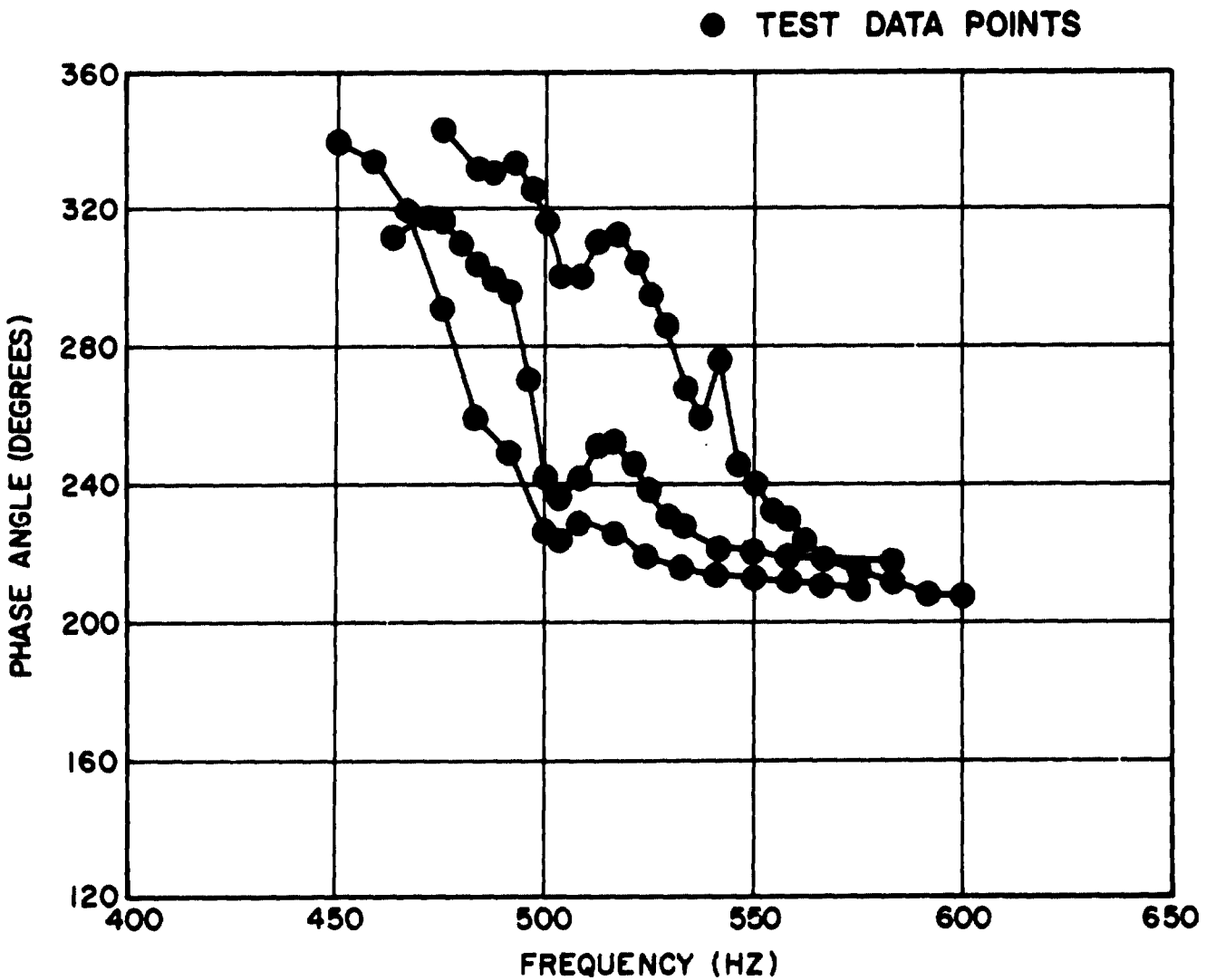

Figure 31. Phase Angle as a Function of Frequency for Amplitude Variation Tests of Ring Cartridge #1 (0.0048 m Wide)

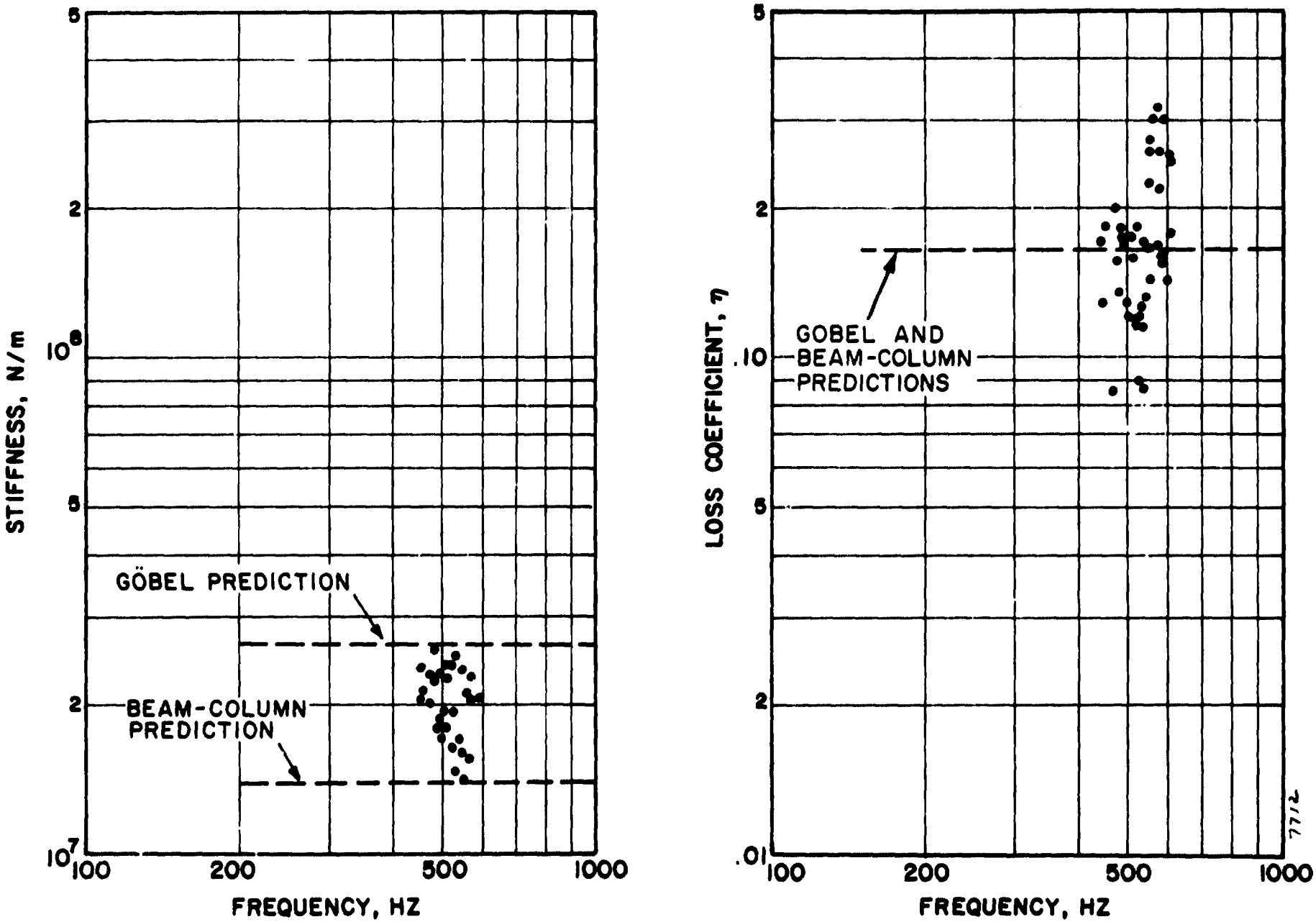

Figure 32. Stiffness and Loss Coefficient of Ring Cartridge #1 (0.0048 m Wide) for Amplitude Variation Tests as a Function of Frequency

TABLE 11

ELASTOMER ROTATING RIG TEST RESULTS AND PREDICTIONS FOR
AMPLITUDE VARIATION TESTS OF RING CARTRIDGE #1 (0.0048 m THICK)

Peak Double Amplitude Strain (m/m)	Stiffness (MN/m)			Damping (MN/m)			Loss Coefficient		
	Average* Measured	Predicted Beam Column	Predicted Göbel	Average* Measured	Predicted Beam Column	Predicted Göbel	Average* Measured	Predicted Variable Strain	Predicted Göbel & Beam Column
.001	23.6	14.0	26.5	3.19	2.290	4.326	0.136	0.14	0.163
.004	19.8	14.0	26.5	3.50	2.290	4.326	0.177	0.21	0.163
.006	17.6	14.0	26.5	3.39	2.290	4.326	0.193	0.23	0.162

*For each change in rotating unbalance

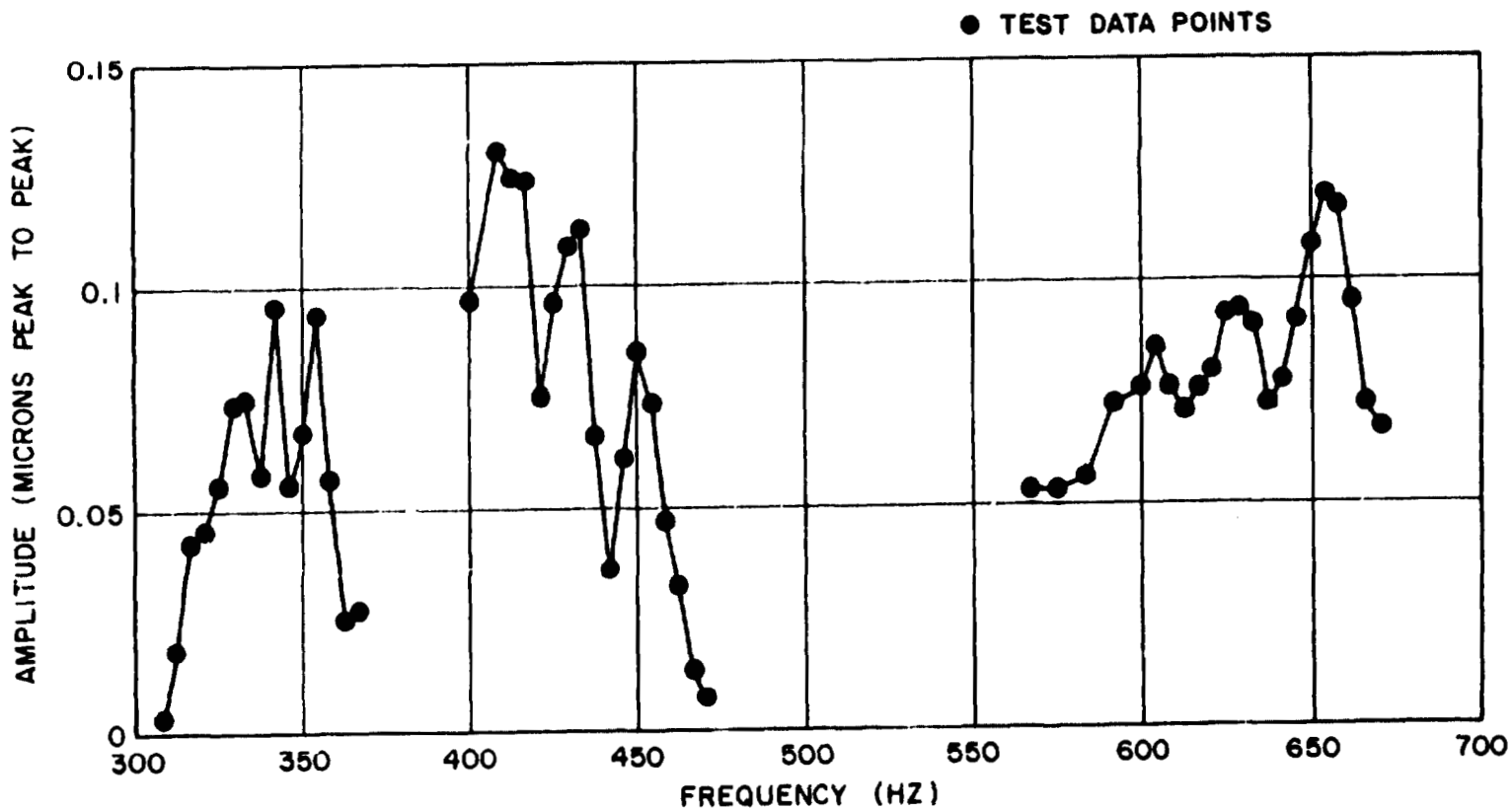

Figure 33. Amplitude Across Elastomer as a Function of Frequency for Ring #2 (0.0024 m Wide)

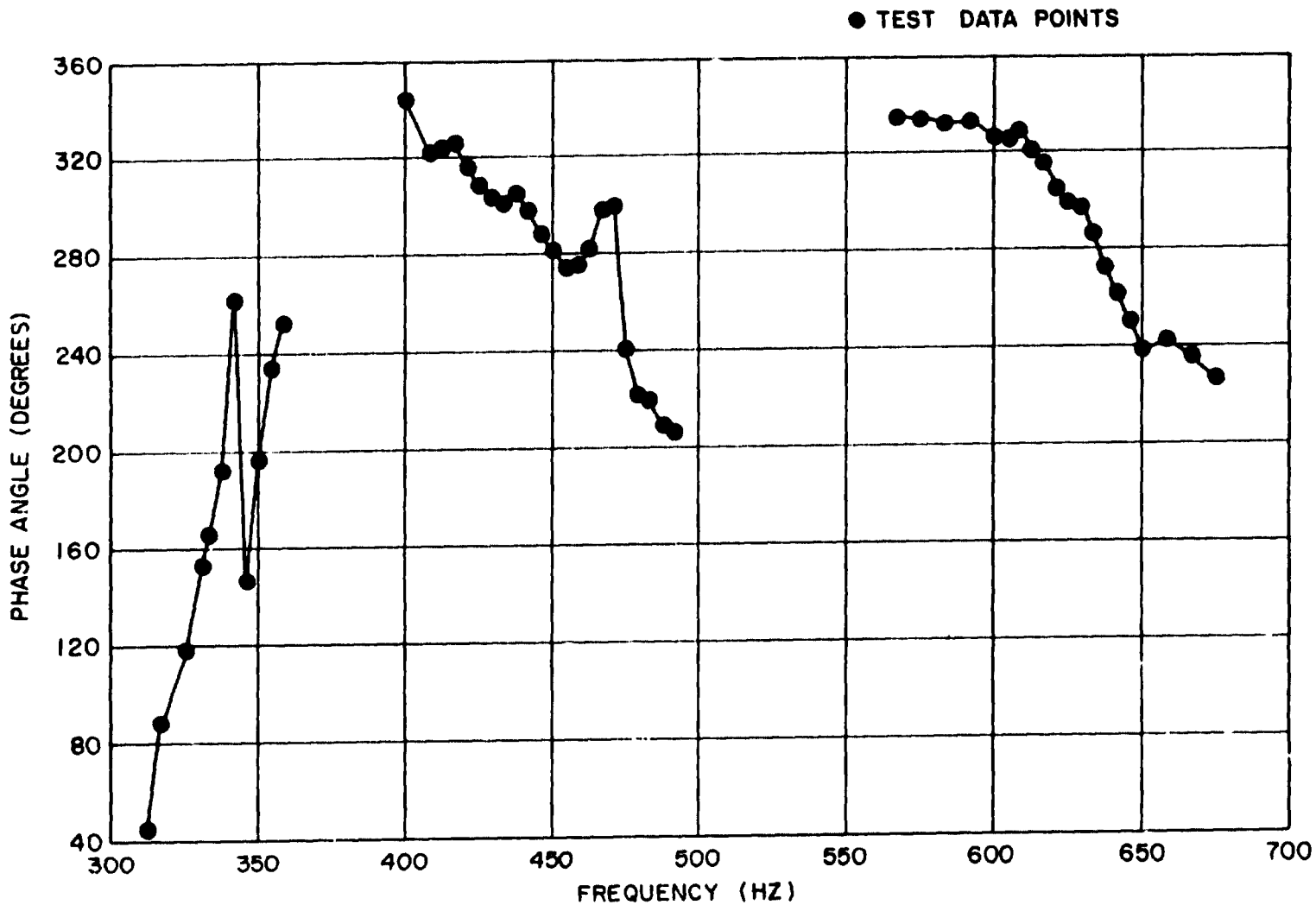

Figure 34. Phase Angle as a Function of Frequency for Ring #2 (0.0024 m Wide)

resonance shows some unexpected behavior, which was not seen in any of the other tests. The sign of the phase angle was reversed from the other tests, and it shifted more than 180 degrees as the speed was increased. It became apparent that the upper housing support flexure resonance (described earlier in this report) was causing this behavior in the data. Although the analysis of this data gives fairly consistent results, it was decided to avoid this speed range (around 20,000 rpm) in subsequent tests. It is noted that the amplitudes for this cartridge were very low and, while within the resolution capability of the capacitance probe, the small signals are expected to have contributed to the scatter in displacement amplitude. In spite of small displacements, the G levels seen by the accelerometers were still of the order of 1 to 10.

The stiffness and loss coefficient values calculated from this data are presented on log-log plots, as functions of speed, in Figure 35. The predicted values of stiffness and loss coefficient, using both Beam-Column and Göbel equations, are shown in Figure 35 for comparison with the test results. Table 12 presents the average measured values of stiffness, damping, and loss coefficient for each of the resonant mass tests, and the predicted values for each, using both Beam-Column and Göbel equations. The test results compare fairly well with the predicted values, particularly those from the Göbel equations. The predicted values for stiffness fall on the edge of and, at some frequencies, just outside the range established by the two prediction methods. For example, at 450 Hz, the measured value of stiffness of 1.361×10^7 N/m compares with the predicted values of 1.302×10^7 N/m from the Göbel equation and 6.87×10^6 N/m from the Beam-Column equation. The predicted values for damping and loss coefficient from the Göbel equation are generally somewhat higher than the measured values. Compare, at 450 Hz, the measured value of damping of 1.923×10^6 N/m with the predicted values of 2.189×10^6 N/m from the Göbel equation and 1.16×10^6 N/m from the Beam-Column equation. The measured loss coefficient at 450 Hz was 0.1413, somewhat lower than the predicted value of 0.169, from both equations. However, this can be explained by the fact that the predictions are based on moderate values of strain (e.g., 0.01) while the value of strain for these tests was very low (about 0.001). For polybutadiene, both damping and loss coefficient are known to fall with low values of strain. From Figure 12, the loss coefficient for a cartridge specimen at a strain of 0.001 would be about 0.14 (by extrapolating the curve) which compares very favorably with the measured value of 0.1413 at 450 Hz.

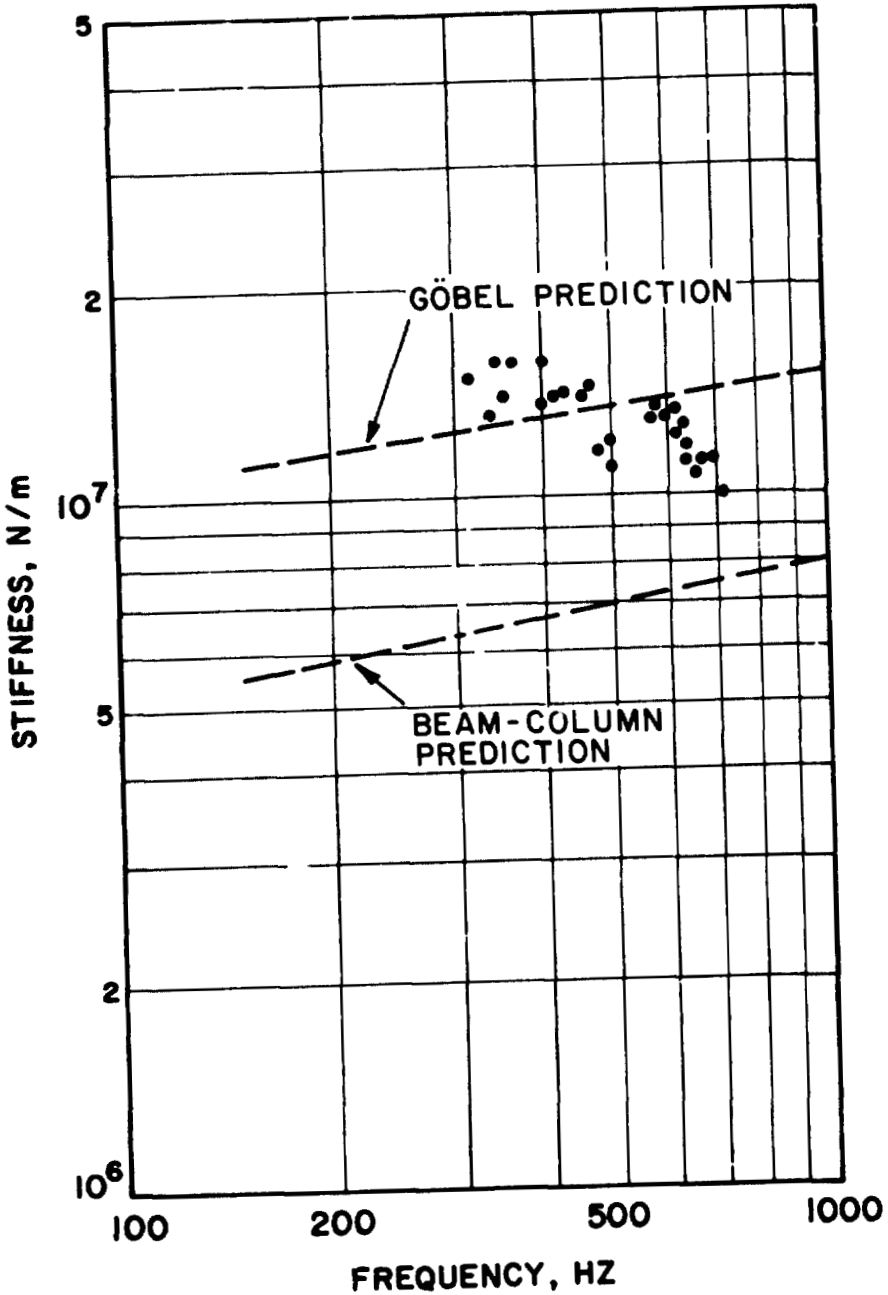

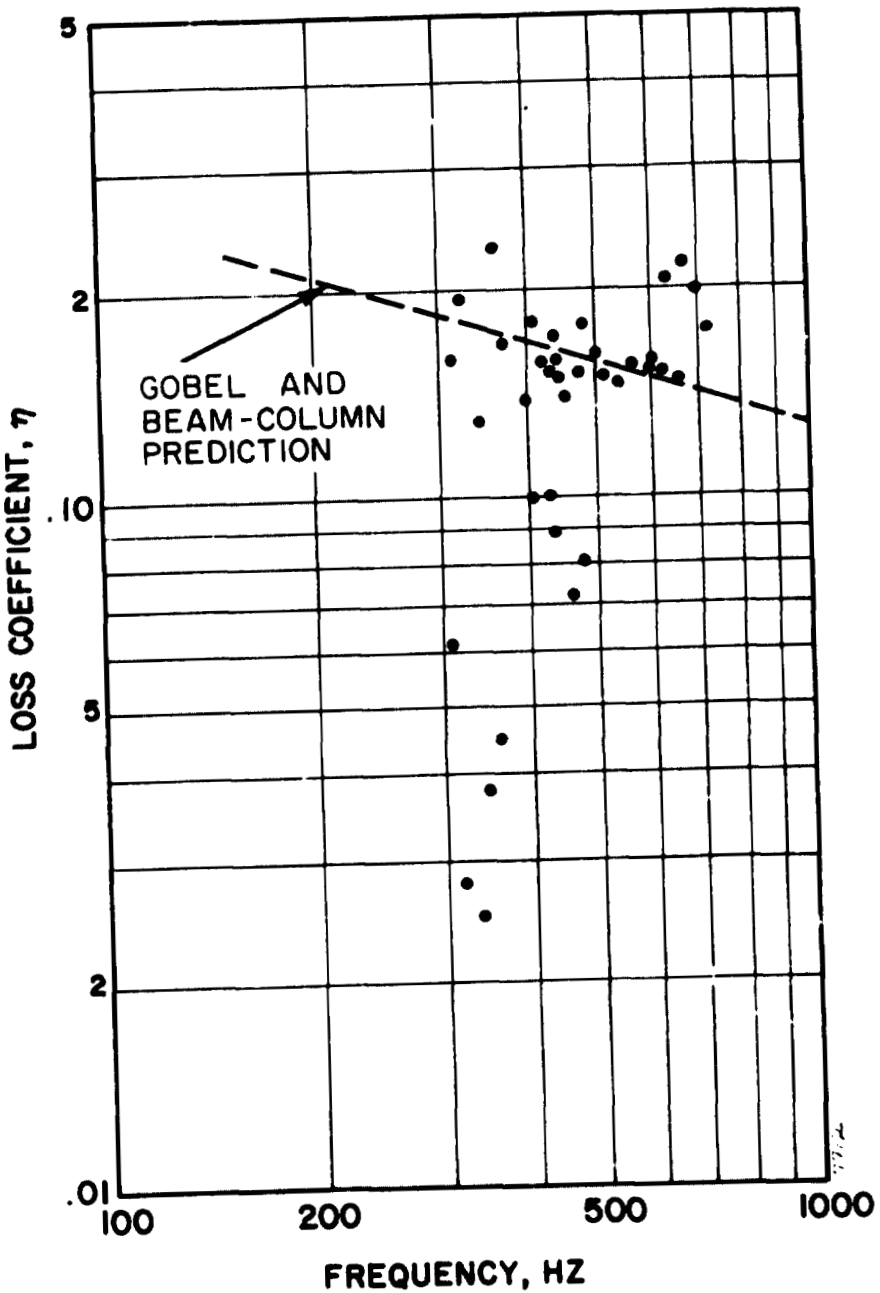

Figure 35. Stiffness and Loss Coefficient of Ring Cartridge #2 (0.0024 m Wide) as a Function of Frequency

TABLE 12

ELASTOMER ROTATING RIG TEST RESULTS AND PREDICTIONS FOR RING CARTRIDGE #2 (0.0024 m WIDE)

Frequency (HZ) Average*	Stiffness (MN/m)			Damping (MN/m)			Loss Coefficient		
	Average* Measured	Predicted Beam Column	Predicted Göbel	Average* Measured	Predicted Beam Column	Predicted Göbel	Average* Measured	Predicted Beam Column	Predicted Göbel
350	14.4	6.5	12.4	1.61	1.20	2.28	0.111	0.183	0.183
450	13.6	6.9	13.0	1.92	1.16	2.19	0.141	0.169	0.169
650	12.6	7.4	14.0	2.08	1.11	2.09	0.172	0.150	0.150

*For each resonant mass

IX. DISCUSSION

The results presented in the preceding section indicate, first, that a rotating load equivalent of the reciprocating load Base Excitation Resonant Mass test method has been successfully implemented and, second, that the predictive methods based on reciprocating elastomer test results are applicable to an elastomer element which is subjected to a rotating load.

Phase angle and amplitude ratio between input and output elements exhibit the same overall variation with frequency as the reciprocating load test method, but, inevitably, the tendency for other motions to superimpose themselves on the desired cylindrical motion introduces additional scatter in the rotating load data.

Considering the resultant difficulties encountered in data interpretation, the comparisons of predicted and measured dynamic properties are encouraging. The predictions of dynamic elastomer stiffness were generally acceptably close to the average measured values. Corresponding predictions of damping or loss coefficient (not accounting for effects of strain) are generally higher than average measured values; this result can be rationalized by considering the known strain dependence of elastomer properties. Unfortunately the elastomer strain levels generated in the rotating load tests were lower than those upon which the elastomer material properties and geometry factors were based. As discussed and demonstrated in Figure 12 (reproduced from reference [3]), reducing strain to low levels clearly reduces damping and loss coefficient; when loss coefficient predictions are extrapolated from Figure 12, they show improved agreement with the rotating load test data.

The nature of these comparisons and the clear importance of strain as a parameter underscore the need, when predicting elastomer dynamic properties for a specific environment, to account for effects of frequency, temperature, amplitude, and material. It is further made clear that a degree of uncertainty is inevitable in any prediction of component properties.

So as to provide qualitative comparison with predictions and measurements of ring cartridge stiffness and damping under a unidirectional load, Figures 36 and 37 are reproduced from reference 3. It has to be pointed out that there

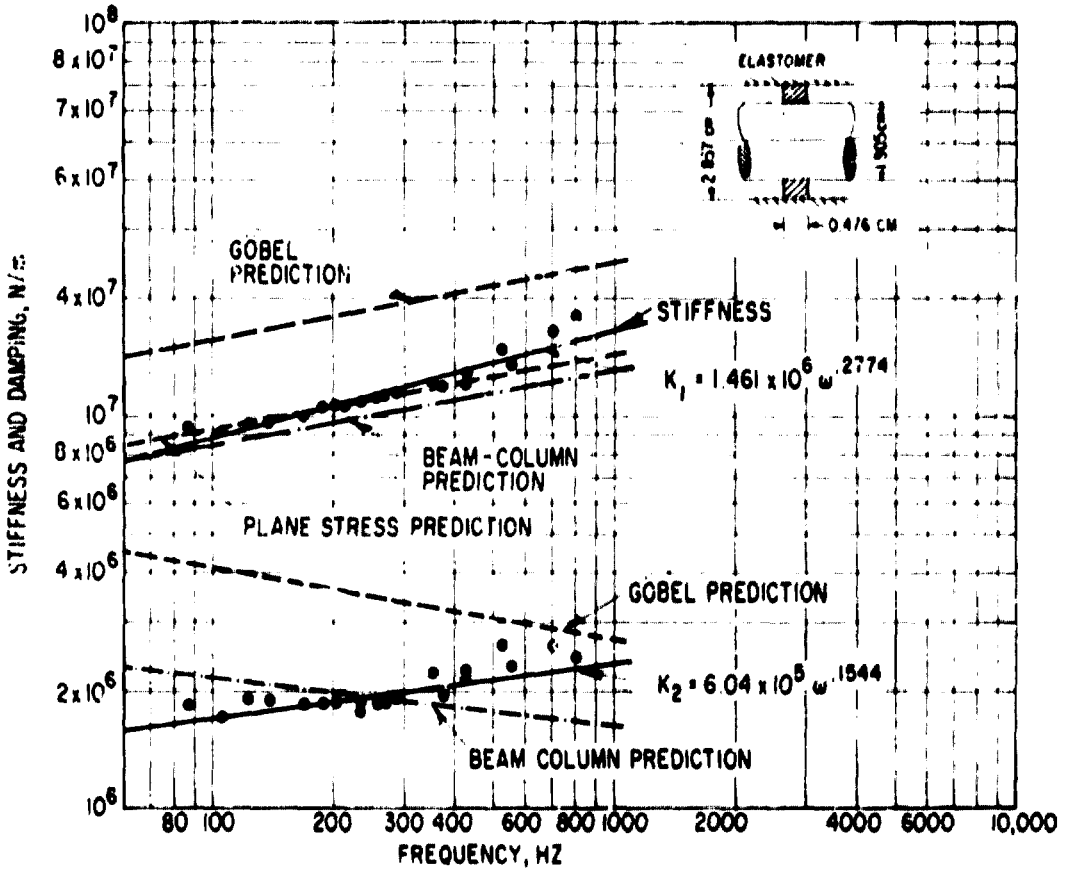

Fig. 36 Stiffness and Damping for Cartridge Specimen. Translational Excitation (from Ref. 3, Fig. 83)

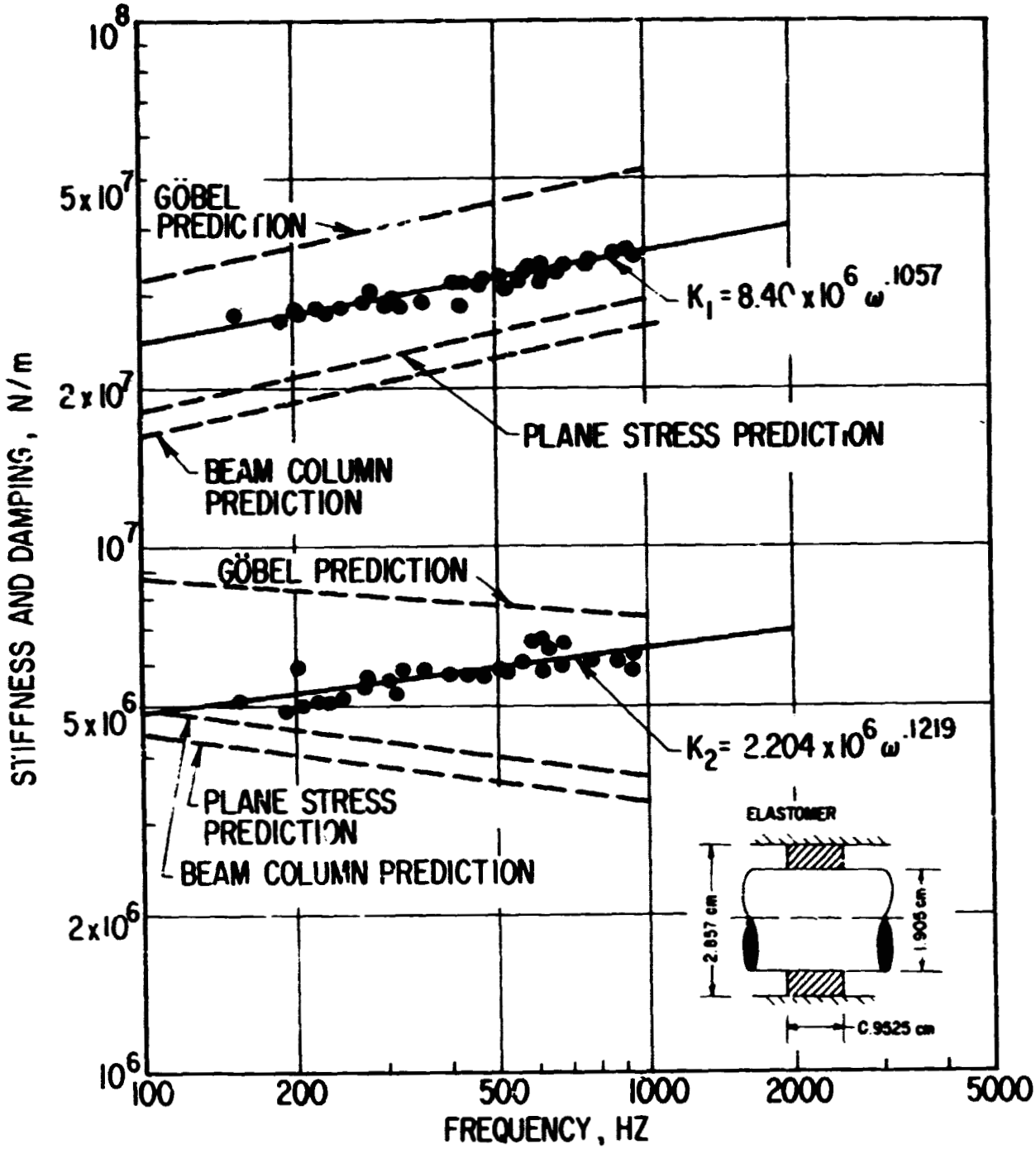

Fig. 37 Stiffness and Damping for Cartridge Specimen. Translational Excitation (from Ref. 3, Fig. 87)

were significant differences in ring dimension for the rotating load tests as opposed to tne unidirectional load tests, as shown in Table 13.

TABLE 13

RING DIMENSIONS FOR UNIDIRECTIONAL LOAD AND ROTATING LOAD TESTS

Load	Ring No.	ID	OD	Length
Unidirectional	1	0.0191	0.0286	0.0048
	2	0.0191	0.0286	0.0095
Rotating	1	0.0635 m	0.073 m	0.0048 m
	2	0.0635 m	0.073 m	0.0024 m

As for the rotating load studies, dynamic characteristics were predicted by the Göbel and the Beam-Column methods, and the measured results tend to fall between the two sets of predictions. However, as a result of the more precise, direct, continuous controllability of the unidirectional test method, the test data is distinctly more consistent than for the rotating load case.

This qualitative comparison of the two test methods adds weight to the conclusion that the dynamic characteristics of an elastomer damper for rotating load applications can be predicted from unidirectional load material data and verified by unidirectional component tests. Apparent inconsistencies in the rotating load application will be a result of the complexities of the rotor-bearing system rather than changes in component properties.

Since the rotating load test rig involved response of a rotor-bearing system to unbalance, it may be regarded as having demonstrated the control of rotating machinery vibrations by an elastomer. The significance of the uncertainties in damping may be viewed within the framework of their influence on the dynamic response of a machine to dynamic excitation. Since average measured stiffness was generally in good agreement with predictions, it is to be expected that confidence in critical speed predictions should be as high as with any other flexible bearing mount. Since, in some cases, predicted damping could be 50 percent low, it must be recognized that, if the elastomer is the only source of damping, then a design should be tolerant to response amplitudes which are a factor of two higher than predicted for nominal conditions. Since uncertainty of a similar magnitude can be expected in squeeze film damper predictions,

the elastomer damping predictions demonstrated within the present report qualify elastomer dampers for application, test, and evaluation, at least on the basis of predictability. The need for application, test, and evaluation of elastomer dampers is clearly indicated. Such evaluation should seek to test, on a rational basis, the ability of elastomer dampers to control machinery vibrations.

X. REFERENCES

1. Chiang, T., Tessarzik, J. M., and Badgley, R. H., "Development of Procedures for Calculating Stiffness and Damping Properties of Elastomers in Engineering Applications. Part I: Verification of Basic Methods", NASA Contractor Report No. CR-120965, prepared by Mechanical Technology Incorporated for NASA-Lewis Research Center under Contract No. NAS3-15334, March 1972.

2. Gupta, P. K., Tessarzik, J. M., and Cziglenyi, L., "Development of Procedures for Calculating Stiffness and Damping Properties of Elastomers in Engineering Applications. Part II: Elastomer Characteristics at Constant Temperature", NASA Contractor Report No. CR-134704, prepared by Mechanical Technology Incorporated for NASA-Lewis Research Center under Contract No. NAS3-15334, April 1974.

3. Smalley, A. J. and Tessarzik, J. M., "Development of Procedures for Calculating Stiffness and Damping Properties of Elastomers in Engineering Applications. Part III: The Effects of Temperature, Dissipation Level, and Geometry", NASA Contractor Report No. CR-134939, prepared by Mechanical Technology Incorporated for NASA-Lewis Research Center under Contracts No. NAS3-15334 and NAS3-18546, November 1975.

4. Göbel, E. F., Berechnung und Gestaltung von Gummifedern, Springer-Verlag, Berlin/Göttengen/Heidelberg, 1955.